Pharmacological Research 215 (2025) 107743

Contents lists available at ScienceDirect

Pharmacological Research

journal homepage: www.elsevier.com/locate/yphrs

PTPRG-AS1 regulates the KITLG/KIT pathway through the ceRNA axis to promote the malignant progression of gastric cancer and the intervention effect of Compound Kushen injection on it

Chao Wu [a,b,1], Yifei Gao [a,1], Zhengsen Jin [a,1], Zhihong Huang [a,c,d,1], Haojia Wang [a], Shan Lu [a], Siyu Guo [a], Fanqin Zhang [a], Jingyuan Zhang [a], Jiaqi Huang [a], Xiaoyu Tao [a], Xinkui Liu [a,e], Xiaomeng Zhang [a], Leiming You [f,*], Qinglin Li [g,*], Jiarui Wu [a,*]

[a] School of Chinese Materia Medica, Beijing University of Chinese Medicine, Beijing 102488, China
[b] Department of Pharmacy, Xuanwu Hospital of Capital Medical University, Beijing 100053, China
[c] Beijing Key Laboratory of Protein Posttranslational Modi cations and Cell Function, Department of Biochemistry and Biophysics, School of Basic Medical Sciences, Peking University Health Science Center, Beijing 100191, China
[d] Department of Biochemistry and Molecular Biology, School of Basic Medical Sciences, Peking University Health Science Center, Beijing 100191, China
[e] Innovative Institute of Chinese Medicine and Pharmacy, Shandong University of Traditional Chinese Medicine, Jinan, Shandong Province 250355, China
[f] School of Life Science, Beijing University of Chinese Medicine, Beijing 102488, China
[g] Zhejiang Cancer Hospital, Hangzhou Institute of Medicine (HIM), Chinese Academy of Sciences, Hangzhou, Zhejiang Province 310022, China

ARTICLE INFO

Keywords:
PTPRG-AS1
Hsa-miR-421
KITLG
Gastric cancer
Compound Kushen injection

ABSTRACT

Gastric cancer (GC) is a common malignant tumor with high mortality, recurrence, and metastasis rates. Compound Kushen injection (CKI) combination chemotherapy has been clinically used for the treatment of GC in China for many years, but its underlying mechanisms of action remain unclear. Recent reports have highlighted the important role of the competing endogenous RNA (ceRNA) mechanism of noncoding RNA (ncRNA) and messenger RNA (mRNA) formation in GC and other tumors. This study aimed to investigate the effects of CKI on GC from the ceRNA perspective. We con rmed the inhibitory effect of CKI on GC in mouse models and cell lines. By examining the GC cell lines sensitive to CKI treatment, we developed the CNScore method to analyze the ceRNA network, revealing that the CKI-GC ceRNA network promotes GC proliferation and metastasis through the PTPRG-AS1/hsa-miR-421/KITLG axis. Finally, we constructed GC cell models with PTPRG-AS1 overexpression or knockdown and GC liver metastasis models and found that PTPRG-AS1 can sponge hsa-miR-421, releasing KITLG and promoting GC proliferation and metastasis through the KITLG/KIT pathway. Taken together, CKI can suppress these malignant phenotypes by regulating the PTPRG-AS1/hsa-miR-421/KITLG axis.

Abbreviations: BP, biological process; BSA, bovine serum albumin; CC, cellular component; CCK-8, cell counting kit-8; CD117, tyrosine kinase receptor c-KIT; CeRNA, competing endogenous RNA; CKI, Compound Kushen injection; CNScore, ceRNA network score; DEGs, differentially expressed genes; DElncRNAs, differentially expressed lncRNAs; DEmiRNAs, differentially expressed miRNAs; DEmRNAs, differentially expressed mRNAs; DEPs, differentially expressed proteins; DSS, disease-speci c survival; EdU, 5-Ethynyl-2′-deoxyuridine; ELISA, enzyme-linked immunosorbent assay; EMT, epithelial-mesenchymal transition; ESI, electrospray source ionization; GC, Gastric cancer; GMP, good manufacturing practice; GO, Gene Ontology; HCT, hematocrit; HER2, human epidermal receptor 2; HGB, hemoglobin concentration; IC_{50}, half-maximal inhibitory concentration; IHC, immunohistochemistry; KEGG, Kyoto Encyclopedia of Genes and Genomes; KITLG, kinase receptor-speci c ligand; LncRNAs, Long non-coding RNAs; MET, mesenchymal-epithelial transition; MF, molecular function; MiRNAs, microRNAs; MREs, miRNA response elements; MRNA, messenger RNA; NC, si-negative control; NcRNA, noncoding RNA; NEU, number of neutrophil; NMPA, the National Medical Products Administration; NSG, NOD-Prkdcscid-IL2Rγ-null; OD, optical density; OS, overall survival; PCT, platelet speci c volume; PFA, paraformaldehyde; PFI, progression free interval; PLT, platelet; PPI, protein-protein interactions; PTPRG-AS1, Protein tyrosine phosphatase, receptor type G, antisense; QPCR, quantitative polymerase chain reaction; RBC, red blood cell; RT-qPCR, reverse transcription quantitative polymerase chain reaction; SCF, stem cell factor; SRB, Sulforhodamine B; SsGSEA, single sample Gene Set Enrichment Analysis; TCA, trichloroacetic acid; TCM, traditional Chinese medicine; TMT, tandem mass tag; TUNEL, terminaldeoxynucleotidyl transferase mediated dUTP nick-end labeling; UPLC-Q/TOF-MSE, Ultra performance liquid chromatography with quadrupole time-of- ight tandem mass spectrometry in MSE centroid mode; WBC, white blood cell; WT, wild-type; MRI, magnetic resonance imaging.

* Corresponding authors.
E-mail addresses: youleiming@bucm.edu.cn (L. You), qinglin200886@126.com (Q. Li), exogamy@163.com (J. Wu).
[1] These authors contributed equally.

https://doi.org/10.1016/j.phrs.2025.107743
Received 6 March 2025; Received in revised form 12 April 2025; Accepted 16 April 2025
Available online 16 April 2025

1. Introduction

Gastric cancer (GC) is a highly malignant tumor and one of the leading causes of cancer-related deaths worldwide [1,2]. In China, GC contributes signi cantly to the overall cancer mortality rate. Radical surgical resection is the most effective approach for extending patient survival [3,4]. Unfortunately, the majority of GC patients are diagnosed at advanced stages, missing the optimal window for surgical intervention. Consequently, metastasis and recurrence are the primary factors leading to mortality in GC patients [5–8]. Hence, the objectives of treatment for patients with advanced GC have shifted toward enhancing the feasibility of surgical resection, mitigating metastasis and postoperative recurrence, and optimizing treatment ef cacy. Presently, a range of treatment modalities, including neoadjuvant, adjuvant, and perioperative chemotherapy, are employed to achieve these goals [9]. While there are reports suggesting that emerging treatment methods, such as the selective implementation of systemic chemotherapy, human epidermal growth factor receptor 2 (HER2)-targeted therapy, antiangiogenic drugs, and immune checkpoint inhibitor therapy, may enhance the ef cacy of GC treatment strategies, these approaches exhibit low response rates and provide bene ts to only a minority of patients [6,8,10–12]. The optimal treatment strategy for patients with GC and the inherent heterogeneity of GC remain to be determined [9]. The challenges associated with investigating the pathogenesis and molecular biomarkers of GC, as well as achieving a comprehensive understanding and enhancing treatment strategies for GC, have yet been fully addressed [9,13,14].

Traditional therapies, such as traditional Chinese medicine (TCM), have a long history of clinical use in China and are recognized as alternative or complementary therapies by medical professionals globally [15–17]. Compound Kushen injection (CKI), a proprietary antitumor drug, has been approved for marketing by the National Medical Products Administration (NMPA). It is manufactured through a good manufacturing practice (GMP) production process and is derived from the roots of two medicinal plants, Kushen (*Radix sophorae avescens*) and Baituling (*Rhizoma heterosmilacis*) [18]. CKI contains bioactive alkaloids such as matrine, oxymatrine, and oxyphorocarpine and has been used in the clinical treatment of various cancers, particularly in digestive system tumors such as GC [18–26]. Mechanistically, CKI promotes autophagy in non-small cell lung cancer through the PI3K/Akt/mTOR pathway and enhances sensitivity to ge tinib [27]. In liver cancer, CKI can alter the immune microenvironment, promote M1 macrophage polarization, and enhance tumor cytotoxicity. Combining CKI with low doses of sorafenib effectively inhibits liver cancer growth and recurrence [28]. In addition, CKI can balance TGF-β/Smad7 signalling in hepatic stellate cells to prevent liver cancer [29]. Although the effectiveness of CKI as an adjuvant therapy for GC is widely recognized, additional research is needed to understand its impact on GC and its mechanism of action [25].

Mammalian genomes have two main gene categories: protein-coding RNA (including messenger RNA, mRNA) and noncoding RNA (ncRNA). Previously, ncRNA was considered useless "noise" while mRNA was considered dominant [30,31]. However, ncRNAs have been found to have various biological functions and play a signi cant role in cancer development [32–34]. Long non-coding RNAs (lncRNAs) and microRNAs (miRNAs) are the two major classes of ncRNAs that were mostly studied and their regulatory mechanisms understood [32,34]. Most ncRNAs use base pairing to selectively bind to and act on other nucleic acids, and competing endogenous RNA (ceRNA) is a typical representative of this mode of action. For example, miRNAs, lncRNAs and mRNAs all share miRNA response elements (MREs), leading to the formation of a ceRNA mechanism in which lncRNAs and mRNAs compete for miRNAs together [34,35]. The ceRNA network supports a wide regulatory range and strong regulatory ability of ncRNAs, which mediates multilevel and complex biological functions [36]. Drawing inspiration from traditional therapies, an increasing number of researchers have discovered that numerous traditional Chinese medicines, natural drugs, or their monomeric compounds are capable of modulating disease progression through interactions with ncRNAs, either individually or as part of a network [37–39]. CeRNA networks are often predicted based on mRNA enrichment analysis, but this approach overlooks the in uence of ncRNAs. In addition, the interaction between traditional Chinese medicine and ncRNAs is important in disease control, but the relationship between CKI and ncRNAs in GC is unclear.

Our team predicted that the ceRNA network could serve as an important mechanism for CKI intervention in GC at a computational level [40]. Additionally, our ndings suggest that the pharmacological effects of CKI intervention in GC may be associated with epithelial-mesenchymal transition (EMT) [41]. This study is an in-depth exploration of our team's early ndings. We rst veri ed the pharmacological effect of CKI on GC using mouse models and cell lines. Subsequently, we proposed the ceRNA network score (CNScore) method to incorporate mRNA and ncRNA information when used in omics data analysis to achieve a comprehensive analysis in which all factors account for the analysis weight. Finally, based on the analysis of the hub CKI-GC ceRNA network, we designed *in vivo* and *in vitro* experiments to verify the mechanism of CKI intervention in GC.

2. Materials and methods

2.1. Detection of the Ingredients of Compound Kushen Injection (CKI)

CKI (batch numbers: 20200329, 20210526 and 20220116) was supplied by Zhendong Pharmaceutical Co., Ltd. (Shanxi, China). Ultra performance liquid chromatography with quadrupole time-of- ight tandem mass spectrometry in MSE centroid mode (UPLC-Q/TOF-MSE) was performed on a Waters HSS T3 UPLC C18 analytical column (100 mm × 2.1 mm, 1.8 μm, Milford, MA, United States). The oven was set at 40 °C; the injection volume was 2 μL; the ow rate was set at 0.4 mL min^{-1}; the mobile phase in positive ion mode consisted of acetonitrile (A: 0.1 % formic acid and 5 mM ammonium formate) and water (B: 0.1 % formic acid and 5 mM ammonium formate); the mobile phase in negative ion mode was consisted of 0.01 % formic acid in acetonitrile (A) and 0.01 % formic acid in water (B). The elution program was as follows: 1 % A for 0–3 min, 1–4 % A for 3–12 min, 4–6 % A for 12–17 min, 6–65 % A for 17–30 min, and 65–100 % A for 30–34 min. The ion source used was electrospray source ionization (ESI) and the temperature was 120 °C. Mass spectrometry (Waters Xevo G2 Q/TOF) was performed in both positive and negative ion modes. The capillary voltage was 2.5 kV (-2.5 kV). The cone voltage was 40 V (-30 V). The desolvation temperature was 500 °C, and the ow rate of 900 L h^{-1}. The cone gas ow rate was 50 L h^{-1}. The scan range was *m/z* 50–1200. The data were acquired in TOF-MSE mode with low collision energy (0 V) and high collision energy (15–55 eV). The data were analyzed utilizing Waters UNIFI software and were integrated with the research reports.

2.2. Cell lines, culture conditions and drug treatment

Human GC cell lines (AGS, HGC-27, MKN-45), a murine GC cell line (MFC), and HEK293T cells were purchased from Procell Life Science & Technology Co., Ltd. (Wuhan, China). Human GC cell line (MKN-74) and normal human gastric epithelial mucosa cell line (GES-1) was obtained from Meisen Cell Technology Co., Ltd. (Zhejiang, China). All cell lines were authenticated by STR pro ling and veri ed to be free of mycoplasma contamination. AGS cells were cultured in Ham's F-12 medium (Corning, USA) supplemented with 10 % fetal bovine serum (FBS, Corning, USA), and HEK293T cells were cultured in DMEM (Corning, USA) supplemented with 10 % FBS, while the other cells were cultured in RPMI 1640 medium (Corning, USA) supplemented with 10 % FBS. All of the cells were cultured in a saturated humidity environment at 37 °C and 5 % CO_2. CKI (batch numbers: 20200329, 20210526 and 20220116; total alkaloid concentration of 25 mg mL^{-1}) was supplied by Zhendong Pharmaceutical Co., Ltd. (Shanxi, China), and 5- uorouracil (5-FU,

batch number: FA211108) was purchased from Shanghai Xudong Haipu Pharmaceutical Co., Ltd. (Shanghai, China). Various concentrations of CKI were added directly to the cell culture medium for drug treatment.

2.3. Homotransplantation of mice

In the experiment involving the formation of subcutaneous tumors, male strain 615 mice (5–7 weeks old, weighing 18–22 g, animal certificate number: SCXK 2020–0001) were purchased from the Institute of Hematology, Chinese Academy of Medical Sciences (Tianjin, China), and they were kept in an SPF environment with experimental animal welfare care. After disinfection, 615 mice were inoculated subcutaneously with MFC cell suspensions ($1 \times 10^7 \times 200\,\mu L^{-1}$) in the right armpit. The long diameter (a) and short diameter (b) of the tumors were measured to calculate the subcutaneous tumor volume using the formula $V = 0.5 \times a \times b^2$. Once the subcutaneous tumor volume exceeded 100 mm^3, the GC model was deemed successful. The model mice were randomly divided into the vehicle (control, sterilized saline water), 5-FU ($25\,mg\,kg^{-1}$) and other different treatment groups. According to the body surface area conversion method, the dose administered to the mice ($65\,mg\,kg^{-1}$) was equivalent to the maximum daily dose administered in human clinical trials. The body weights and subcutaneous tumor volumes of the mice were measured every 3 days. Finally, the mice were sacri ced, and the subcutaneous tumor tissues were removed, and their weight and volume were determined. Then, H&E staining, immunohistochemistry (IHC) staining, TUNEL assay, ow cytometry, RT-qPCR and Western blotting assays were applied to the tumor tissues. Cytometry was executed using a hemocytometer. Subsequently, the serum from the mice was subjected to ELISA. This animal experiment was approved by the Animal Ethics Committee of Beijing University of Chinese Medicine (Ethics number: BUCM-2022010502-1130).

2.4. Xenotransplantation of mice

In the experiment involving the formation of liver metastatic tumors, male immunode cient NSG (NOD-Prkdcscid-IL2Rγ-null) mice (5–6 weeks old, weighing 18–22 g, animal certi cate number: SCXK 2021-0010) were purchased from Beijing Viewsolid Biotechnology Co., Ltd. (Beijing, China), and they were housed in an SPF environment with experimental animal welfare care. In the CKI pharmacodynamics experiment, a liver metastasis model was created by injecting 1×10^6 HGC-27 wild-type (WT) cells into the hepatic portal vein of NSG mice. Magnetic resonance imaging (MRI) was used to con rm whether metastatic tumors had formed in the liver. The mice with liver metastases were randomly divided into model and different treatment groups (Fig. 10A). MRI was used to observe changes in the liver metastases throughout the process of CKI intervention. The mice were then euthanized, and the livers were subjected to H&E staining, IHC staining, RT-qPCR and western blotting. Whole blood was used for blood cell counts, and serum was prepared for ELISA. As mentioned above, other experiments aimed to observe the function of the PTPRG-AS1 gene (Fig. 8A and G). To achieve this goal, HGC-27 cells (1×10^6 cells per mouse) stably transfected with PTPRG-AS1 overexpression vector or empty vector were injected into the hepatic portal vein of NSG mice. Similarly, for all knockdown experiments, MKN-45 cells (3×10^5 cells per mouse) transduced with lentiviruses expressing PTPRG-AS1 shRNA (sh-PTPRG-AS1) or negative control shRNA (sh-NC) were injected into the hepatic portal vein of NSG mice. MRI was used to monitor the occurrence of liver metastasis *in vivo*. After 30 days, all of the mice were euthanized, and subsequent experiments similar to those described above were performed. This animal experiment was approved by the Animal Ethics Committee of Beijing University of Chinese Medicine (Ethics number: BUCM-2023020302-1127).

2.5. Reverse transcription quantitative polymerase chain reaction (RT-qPCR) analysis

An RNA Easy Fast Cell Kit (Tiangen, China) was used for total RNA isolation according to the manufacturer's instructions. The quality of the total RNA was determined by a SpectraMax Quick Drop reader (Molecular Devices, USA). Total RNA (1 μg) was used for cDNA synthesis of long RNA (mRNA and lncRNA) following the instructions of the ReverTra Ace qPCR RT Kit (Toyobo, Japan). Additionally, the Bulge-Loop miRNA Starter Kit (Ribobio, China) was employed to reversely transcribe miRNA into cDNA according to the manufacturer's protocols. Quantitative polymerase chain reaction (qPCR) was performed to measure the relative expression of long RNAs (mRNA and lncRNA) or miRNAs, using SYBR Green Realtime PCR Master Mix (Toyobo, Japan) with the QuantStudio 6 Flex (Applied Biosystems, USA). GAPDH or β-actin was used as a control and the $2^{-\Delta\Delta Ct}$ method was used for the data analysis. The primers for the target genes were synthesized by Sangon Biotech Co., Ltd. (Shanghai, China) and their sequences are listed in the Supplementary Methods.

2.6. Western blot

Tumor tissues or GC cells were collected in RIPA lysis buffer supplemented with Protease and Phosphatase Inhibitor Cocktail (Beyotime, China). The collected samples were then centrifuged at 13,000 rpm and 4 °C for 10 min. The supernatants were preserved and used for western blot analysis. The total protein concentration was measured with a BCA Protein Assay Kit (Solarbio, China). Total protein (20 μg) was mixed with 5 × sample buffer, boiled at 99 °C for 5 min and loaded onto 10 % SDS-PAGE gels. Then the protein bands were transferred onto NC membranes and blocked with 5 % nonfat milk or 5 % bovine serum albumin (BSA) for 2 h at room temperature. The NC membranes with proteins were incubated with diluted primary antibodies (Abcam, USA; Af nity or Proteintech, China) at 4 °C overnight, including anti-KITLG (Abcam, USA, ab64677, 1:5000), anti-KIT (Abcam, USA, ab32363, 1:1000), anti-phospho-KIT (Af nity, China, AF3153, 1:1000), anti-PIK3R1 (Proteintech, China, 60225–1-Ig, 1:500), anti-phospho-PIK3R1 (Af nity, China, AF3241, 1:1000), anti-AKT (Proteintech, China, 10176–2-AP, 1:1000), anti-phospho-AKT (Proteintech, China, 66444-1-Ig, 1:1000), anti-GSK-3β (Proteintech, China, 22104-1-AP, 1:1000), anti-phospho-GSK-3β (Af nity, China, AF2016, 1:1000), anti-Cyclin D1 (Proteintech, China, 26939-1-AP, 1:1000), anti-c-Myc (Proteintech, China, 10828-1-AP, 1:1000), anti-β-catenin (Proteintech, China, 51067.2-AP, 1:3000), anti-E-cadherin (Proteintech, China, 20874.1-AP, 1:1000), anti-N-cadherin (Proteintech, China, 22018.1-AP, 1:1000), anti-Vimentin (Proteintech, China, 10366.1-AP, 1:3000), and anti-GAPDH (1:5000) antibodies. Then, the membranes were incubated with relative sources of secondary antibodies (1:5000) at room temperature for 2 h. Finally, the speci c protein bands were visualized with Immobilon Western Chemiluminescent HRP Substrate (Millipore, Sigma, USA). ImageJ software was used for image analysis and the signals of speci c proteins were normalized to those of GAPDH.

2.7. Immunohistochemistry (IHC), terminaldeoxynucleotidyl transferase mediated dUTP nick-end labeling (TUNEL), and enzyme-linked immunosorbent assay (ELISA)

The tumor tissues were xed in 4 % paraformaldehyde (PFA) for 48 hours, embedded in paraf n and sectioned. Tumor tissue sections underwent a series of procedures, including dewaxing, immersion in H_2O_2 solution, antigen retrieval (citrate buffer, pH = 6.0), blocking, incubation with speci c primary antibodies (Abcam, USA; Proteintech, China), incubation with secondary antibodies, washing, staining with DAB reagent (Abcam, USA), and counterstaining with hematoxylin, to obtain the nal IHC sections. The TUNEL assay was conducted by staining tumor tissue sections with the In Situ Cell Death Detection Kit,

POD (Roche, Switzerland) following the instructions provided by the manufacturer, and the results of staining were subsequently observed using a confocal microscope (Nikon, Japan). The concentrations of the target proteins in the serum of the mice was determined using a Mouse KITLG ELISA Kit (Proteintech, China), Mouse CA19–9 ELISA Kit, Mouse CA72–4 ELISA Kit, and Mouse CEA ELISA Kit (Myhalic, China) in accordance with the manufacturer's instructions. Image Pro Plus software was used for image data analysis.

2.8. Flow cytometry

The fresh tumor tissues or spleens of the mice were cut into small pieces, and a single cell suspension was subsequently obtained after digestion in 0.5 mg mL^{-1} collagenase IV (Sigma, USA) supplemented with 0.15 mg mL^{-1} DNase I (Sigma, USA), ltration through a 70 μm cell strainer, and erythrocyte lysis. First, 1000 μL of Ghost Dye™ Violet 510 (1:1000) was added to each 100 μL of single cell suspension and incubated at room temperature for 15 min in the dark. Second, 1 μg of TruStain FcX™ (anti-mouse CD16/32) was added to each sample and incubated at room temperature for 15 min in the dark. Third, a mixture of BB515 rat anti-mouse CD45 (BD, USA), APC/Fire™ 750 anti-mouse CD3, APC anti-mouse CD4, and PE/Cyanine7 anti-mouse CD8a (BioLegend, USA) antibodies was incubated with the samples at room temperature for 20 min in the dark. Finally, the samples were detected using ow cytometry (Cytek, USA), and FlowJo software was used to analyze the data.

The cells undergoing apoptosis were detected with the FITC Annexin V Apoptosis Detection Kit I (BD, USA). Brie y, the collected cells were stained with FITC Annexin V for 15 min, followed by staining with PI for 5 min. Then, ow cytometry was used to analyze the stained cells. Determination of the cell cycle distribution of the GC cells was conducted through ow cytometry, using a Cell Cycle Analysis Kit (Beyotime, China). Every sample was stained with a mixed buffer (500 μL of staining buffer, 25 μL of PI, and 10 μL of RNase A) at 37 °C for 30 min. All of the aforementioned procedures were conducted in a dark environment. These experiments were carried out independently three times.

2.9. Dual-luciferase reporter assay

The dual-luciferase reporter assay was performed as previously described [42]. The sequences of PTPRG-AS1 and KITLG-3' untranslated region (3' UTR) and their corresponding mutations were designed, synthesized and inserted into luciferase reporter vector pSI-Check2 (HanBio, China), termed PTPRG-AS1-WT, PTPRG-AS1-MUT, KITLG-3' UTR-WT and KITLG-3' UTR-MUT, respectively. All constructs were con rmed by sequencing. MKN-45 and HGC-27 cells were seeded in a 96-well plate at a density of 4×10^4 or 1×10^4 cells per well, respectively, for 24 h before transfection. The cells were co-transfected with a mixture of luciferase reporter vectors and miRNA mimics or inhibitor (RiboBio, China) to examine the miRNA binding ability. At 48 h post-transfection, the relative luciferase activity was measured using a dual-luciferase reporter assay system (Beyotime, China) following the manufacturer's protocol. At least three replicates with three independent biological experiments were performed, and the results were normalized to re y luciferase. These experiments were carried out independently three times.

2.10. Sulforhodamine B (SRB) assay and cell counting kit-8 (CCK-8) assay

The SRB Cell Proliferation and Cytotoxicity Test Kit (Keygen BioTech, China) was utilized in accordance with the manufacturer's protocol for the CKI ef cacy experiment. Brie y, 1×10^4 cells (AGS, HGC-27, MKN-74, and GES-1) or 4×10^4 cells (MKN-45) were seeded per well in 96-well plates. After CKI intervention, the cells were xed with 16 % trichloroacetic acid (TCA), stained with 4 % SRB, washed with 1 % acetic acid, and dissolved in Trisbase (pH = 10.5). The absorbance was detected by a SpectraMax i3x microplate reader (Molecular Devices, USA) at a wavelength of 515 nm. A CCK-8 Assay Kit (Dojindo, Japan) was used to detect the proliferation ability of the GC cells after transfection. In brief, 10 μL of CCK-8 reagent was added directly to the cell culture medium per well, and the GC cells were routinely incubated for 2–4 h in a cell culture incubator. Subsequently, the absorbance was measured using a SpectraMax i3x microplate reader (Molecular Devices, USA) at a wavelength of 450 nm. These experiments were carried out independently three times.

2.11. 5-Ethynyl-2′-deoxyuridine (EdU) incorporation assay

An EdU incorporation assay was conducted to evaluate the proliferation of the GC cells. An EdU Cell Proliferation Kit with Alexa Fluor 488 (Beyotime, China) was used in accordance with the manufacturer's protocol. Brie y, AGS (1×10^5 cells), HGC-27 (2×10^5 cells), and MKN-45 (4×10^5 cells) cells were inoculated into a confocal dish and subjected to routine culture for 24 h before being intervened with the relevant test factors. After the intervention, the cells were incubated with 10 μM EdU for 2 h, and then the cells were xed with 4 % PFA for 15 min. The xed cells were washed with 3 % BSA for 5 min, permeabilized with 0.3 % Triton X-100 for 20 min, stained with Click Reaction Buffer in the dark for 30 min, stained with Hoechst 33342 in the dark for 15 min, and washed with PBS for 5 min before uorescence images were acquired using a FLUOVIEW FV3000 confocal microscope (Olympus, Japan). The data were analyzed using ImageJ software.

2.12. Colony formation assay

Various GC cell lines (500 cells per well), with or without relevant intervention factors to be tested, were seeded onto 6-well plates and routinely cultured for 15 d. On the last day, the GC cells were xed with 4 % PFA for 20 min and stained with 1 % crystal violet for 3 min. The colonies were subsequently counted and analyzed utilizing ImageJ software. These experiments were carried out independently three times.

2.13. Cell migration, cell invasion and cell adhesion assays

For the cell migration assay, the AGS (2×10^4 cells per Transwell), HGC-27 (2×10^4 cells per Transwell), and MKN-45 (1×10^5 cells per Transwell) cells were routinely digested, suspended in serum-free medium, and seeded onto the upper chamber of Transwell inserts (8 μm; Corning, USA) in 24-well plates. Meanwhile, the bottom chamber was lled with complete medium. Following a 24-h culture (a 48-h culture for the MKN-45 cells), all cells were xed with 4 % PFA. Subsequently, the cells in the upper chamber were removed and the cells in the bottom chamber were stained with 1 % crystal violet for 5 min. Finally, the aforementioned cells were imaged using an inverted microscope (Nikon, Japan). The cell invasion assay was conducted in a manner similar to that used for the cell migration assay, with the exception that the upper Transwell chamber utilized in the cell invasion assay was coated with 500 μg mL^{-1} of Matrigel (ABW, China). For the cell adhesion assay, according to the instructions provided by the manufacturer of the Matrigel, the Matrigel concentration was adjusted to 5 mg mL^{-1} using PBS and then used to coat a 24-well plate. The plate was then incubated at a temperature of 37 °C for 2 h. Following a 48-h CKI intervention, the AGS (2×10^5 cells per well), HGC-27 (2×10^5 cells per well), and MKN-45 (4×10^5 cells per well) cells were routinely digested and subsequently transferred to the 24-well plate that had been coated with Matrigel. After 24 h, the cells were xed with 4 % PFA, stained with SRB, and washed with PBS. Finally, the absorbance of the samples was detected using the SpectraMax i3x microplate reader (Molecular Devices, USA) at 515 nm.

2.14. Transient transfection

For oligonucleotide transfection, prior to transfection, HGC-27 cells (4×10^5 cells per well) and MKN-45 cells (8×10^5 cells per well) were seeded in 6-well plates and cultured for 24 h. The si-PTPRG-AS1 and si-negative control (NC) oligonucleotides were designed and synthesized by GenePharma (Shanghai, China). The hsa-miR-421 mimics, hsa-miR-421 inhibitor, and their respective NC oligonucleotides were designed and synthesized by RiboBio (Guangzhou, China). The transfection media used for the HGC-27 cells and MKN-45 cells were X-tremeGENE siRNA Transfection Reagent (Roche, Switzerland) and Lipofectamine 2000 (Thermo Fisher Scienti c, USA), respectively, in accordance with the manufacturer's instructions. The oligonucleotide sequences used are listed in the Supplementary Methods.

For plasmid transfection, HGC-27 cells and MKN-45 cells were seeded in 6-well plates at the same cell density as above and cultured for 24 h. The plasmid pcDNA3.1-CMV-PTPRG-AS1 was synthesized by Hanbio Biotechnology (Shanghai, China) to overexpress the PTPRG-AS1 gene. According to the manufacturer's instructions, X-tremeGENE HP DNA Transfection Reagent (Roche, Switzerland) and Lipofectamine 2000 (Thermo Fisher Scienti c, USA) were used as transfection media for HGC-27 cells and MKN-45 cells, respectively. All constructs were con rmed by sequencing.

2.15. Lentiviral transduction and stable transfection

To construct a stable overexpression vector for PTPRG-AS1, the full-length cDNA of PTPRG-AS1 was synthesized and inserted into the overexpression vector pHBLV-CMV (HanBio, China). An empty vector lacking the PTPRG-AS1 sequence was utilized as the negative control. To create a stable PTPRG-AS1-knockdown vector, synthesized sequences targeting PTPRG-AS1 or containing a negative control sequence were cloned into the pHBLV vector (HanBio, China), which includes the shRNA sequence. All constructs were con rmed by sequencing. The shRNA sequences are shown in the Supplementary Methods. The vector plasmid overexpressing PTPRG-AS1 or the shRNA plasmid targeting PTPRG-AS1 was stably transfected into the target cells via lentiviral transduction. HEK293T cells (5×10^6 cells per dish) were seeded in 10 cm culture dishes under standard culture conditions before transfection. The lentiviral transfer plasmid encoding the insert of interest was co-transfected with the psPAX2 packaging plasmid and the pMD2G envelope plasmid into HEK293T cells using Lipofectamine 2000 in Opti-MEM (Gibco, USA) to produce lentiviral particles. After 72 h of transfection, the medium containing lentiviral particles was centrifuged at 500 g at 4 °C for 15 min. The harvested lentiviral particles were ltered through 0.45 μm PVDF membranes (Millipore, USA) and stored at −80 °C. Puromycin (1.5 μg mL^{-1} and 3.5 μg mL^{-1}) was used to screen the stably transfected HGC-27 cells and MKN-45 cells, respectively.

2.16. Bioinformatics analysis and ceRNA network score (CNScore) analysis

The Gene Ontology (GO, http://geneontology.org/) database, the Kyoto Encyclopedia of Genes and Genomes (KEGG, https://www.kegg.jp/), and the Hallmark gene set of the MSigDB (https://www.gsea-msigdb.org/gsea/msigdb) database were used to perform enrichment analysis of the biological process (BP), cellular component (CC), molecular function (MF), pathway and other biological entries for all differentially expressed genes (DEGs) and differentially expressed proteins (DEPs). The above procedures were implemented using the clusterPro ler package within R software based on the hypergeometric distribution algorithm. P value < 0.05 were considered to indicate statistical signi cance. The Search Tool for the Retrieval of Interacting Genes/Proteins (STRING, https://string-db.org/) was utilized to procure protein-protein interactions (PPI) data. The PPI network and the ceRNA network were constructed using Cytoscape software (version 3.9.1). Subsequently, the network data were subjected to analysis using the cytoHubba and MCODE plug-ins within Cytoscape, respectively. The differential analysis between the two groups was conducted using the limma package in R software. The lncLocator database (http://www.csbio.sjtu.edu.cn/bioinf/lncLocator/) and the lncATLAS database (https://lncatlas.crg.eu/) were used for lncRNA subcellular localization analysis.

As mentioned in the introduction of this study, to annotate the entire ceRNA network with biological meaning, we propose the CNScore method. In brief, we rst collected the relevant intersect genes of CKI at the transcriptional level. We intersected the DEGs between the control group of GC cells and the group of GC cells that underwent CKI intervention, as well as the DEGs between the GC cell group and the normal gastric epithelial cell group. The genes that were common to both sets were used as the CKI regulatory gene set for GC cells. Then, using the starBase database (https://rnasysu.com/encori/), we predicted the ceRNA relationships between lncRNAs, miRNAs, and mRNAs to construct the CKI-GC ceRNA network I. Second, using the cytoHubba plug-in within Cytoscape software to analyze the network, we took the top 50 % of the nodes of four algorithms, including BottleNeck, Degree, EPC, and MCC, and intersected them with CKI-related GC cell proteomic data and human PPI background network nodes from the STRING database. This allowed us to extract the subnetworks and de ne them as the CKI-GC ceRNA network II. Finally, the network was ltered again using molecules with good prognostic signi cance for GC patients and the MCODE plug-in within Cytoscape to obtain the nal hub CKI-GC ceRNA network. The gene expression pro le data and corresponding clinical information of the patients with STAD were downloaded from The Cancer Genome Altas (TCGA, https://portal.gdc.cancer.gov/), and the data were cleaned and organized to obtain a normalized data matrix. A total of 371 tumor samples were obtained by combining samples with both miRNA-seq and RNA-seq data, and a total of 292 samples with complete clinical information were retained. Using the single sample Gene Set Enrichment Analysis (ssGSEA) algorithm in the GSVA package of R software, all nodes (all molecules) in the ceRNA network were used as signature genes to score the TCGA-STAD patient samples obtained above. Then, the survminer package in R software was used to determine the optimal cut-off point using maximally selected rank statistics. This resulted in the division of patients into two groups: the CNSscore High group (175 patients) and the CNSscore Low group (117 patients). The Limma package in R software was used to analyze DEGs between these two groups, with a differential expression threshold set as $|\text{fold change (FC)}| > 1.5$ and p value < 0.05. The Kaplan-Meier method was used to construct survival curves, and the log-rank test was used to evaluate the statistical difference between the CNScore High group and the CNScore Low group. The chi-square test was used to analyze the difference in clinical information between the CNSscore High group and the CNSscore Low group. The *Pearson* correlation test was utilized to conduct correlation analyses. The method for conducting enrichment analysis remains consistent with the aforementioned approach.

2.17. Transcriptomics analyses

Transcriptomic analysis was conducted utilizing ceRNA and miRNA microarray chips. MKN-45 cells and HGC-27 cells were cultured in the presence or absence of 1 mg mL^{-1} CKI for 48 h, while GES-1 cells were left untreated. After RNA extraction, quali cation, and quanti cation were performed on the aforementioned cells, the resulting samples were subjected to detection using an Agilent Human ceRNA Microarray 2019 (Design ID: 086188, Agilent, USA), and an Agilent Human miRNA Microarray Kit (Design ID: 070156, Agilent, USA). The raw RNA microarray chips data were extracted using Feature Extraction software (Agilent, USA). DEGs were identi ed using a t-test to calculate FC and p value. The threshold for DEGs was set at a $|FC=$ of ≥ 2 and a p value of < 0.05. More detailed experimental steps are provided in the Supplementary Methods.

Table 1
Representative compounds in CKI.

No.	Component name	Formula	t_R (min)	Calculated (*m/z*)	Observed (*m/z*)	Mass error (ppm)	MS/MS
1	#N-Methylcytisine	$C_{12}H_{16}N_2O$	2.32	205.1335	205.1334	−0.5	191.1196, 174.0927, 162.0918, 146.0602, 108.0810
2	Cytisine	$C_{11}H_{14}N_2O$	2.68	191.1179	191.1178	−0.5	162.0922, 148.0755, 133.0498, 120.0812
3	#Macrozamin	$C_{13}H_{24}N_2O_{11}$	2.99	429.1351	429.1349	−0.5	311.0985, 191.0571, 149.0439
4	Sophoranol N-oxide	$C_{15}H_{24}N_2O_3$	3.03	281.1860	281.1863	1.1	263.1763, 221.1289, 203.1188, 150.1275, 148.1119, 98.0964
5	Baptifoline	$C_{15}H_{20}N_2O_2$	3.24	261.1598	261.1600	0.8	243.1497, 146.0612, 114.0909, 96.0804
6	#Matrine	$C_{15}H_{24}N_2O$	8.21	249.1961	249.1971	3.9	247.1819, 176.1081, 150.1285, 148.1128, 136.1131, 98.0971
7	#Sophocarpine	$C_{15}H_{22}N_2O$	9.28	247.1805	247.1802	−1.2	179.1538, 150.1269, 148.1115, 136.1113, 98.0954, 96.0799
8	#Sophoridine	$C_{15}H_{24}N_2O$	9.84	249.1961	249.1958	−1.2	176.1068, 152.1427, 148.1159, 136.1113, 120.0801, 98.0594
9	#Oxysophocarpine	$C_{15}H_{22}N_2O_2$	10.47	263.1754	263.1751	−1.1	245.1649, 203.1178, 150.1269, 136.1113, 96.0799
10	Sophoramine	$C_{15}H_{20}N_2O$	10.48	245.1648	245.1647	−0.4	203.1179, 150.1269, 148.1115, 136.1113, 98.0957, 96.0799
11	#Oxymatrine	$C_{15}H_{24}N_2O_2$	11.44	265.1911	265.1904	−2.6	247.1805, 205.1546, 178.1449, 176.0726, 148.0765, 98.0951
12	#Sophoranol	$C_{15}H_{24}N_2O_2$	12.63	265.1911	265.1911	0.0	247.1809, 205.1341, 168.1384, 150.1276, 148.1271, 98.0598
13	#Liriodendrin	$C_{34}H_{46}O_{18}$	20.83	787.2655	787.2658	0.4	741.2589, 579.2067, 417.1543, 181.0500
14	#Trifolirhizin	$C_{22}H_{22}O_{10}$	23.43	491.1184	491.1186	0.4	455.1220, 283.0612

[a]) # indicates validation using compound standards. Information on all 91 compounds is provided in [Supplementary Tables, Table S1].

2.18. Proteomics analyses

HGC-27 and MKN-45 cells were treated with or without 1 mg mL^{-1} CKI treatment for 48 h, and GES-1 cells were subjected to tandem mass tag (TMT) labelling proteomics. Proteome Discoverer 1.4 software (Thermo Fisher Scienti c, USA) was performed for identi cation and quantitation analysis. DEPs were identi ed using a *t*-test to calculate the FC and *p* value. The threshold for DEPs was set at a |FC = of ≥ 1.2 and a *p* value of < 0.05. A detailed description of the method is provided in the Supplementary Methods.

2.19. Statistical analysis

All of the data were statistically analyzed using R software (version 4.2.1) or GraphPad Prism 9.0 software, and the data are presented as *mean* ± *SD*, unless otherwise stated. Some of the statistical methods used for bioinformatics are described in the Methods section on bioinformatics analysis and ceRNA network scoring. Unpaired Student's *t*-test was used to compare the differences between the two groups. One-way analysis of variance (one-way ANOVA) and Tukey's honest signi cant difference (Tukey's HSD) test were used to compare the differences between groups. A *p* value less than 0.05 was considered to indicate statistical signi cance.

3. Results

3.1. A total of 91 compounds including matrine have been identi ed in CKI

To clarify the chemical composition of CKI, UPLC/Q-TOF-MS/MS analysis was carried out and 91 chemical compounds were identi ed (Table 1, Fig. S1A). The result showed CKI contains 51 alkaloids, 7 lignans, 17 avonoids, 3 amino acids, 4 sugars and their derivatives, 6 organic acids, 1 cardiac glycoside, 1 iridoid and 1 alkylphenol. The identi cation results of all compounds in CKI, as well as the representative mass spectra, can be found in Supplementary Table S1 and Fig. S1B-H.

3.2. CKI affects multiple tumor pathophysiological indicators and enhances the anticancer effect of 5-FU in vivo

To examine the intervention effect of CKI on GC, we used strain 615 mice to construct a classical GC mouse model to evaluate the pharmacological effects of CKI. We also established a rst-line chemotherapy (5-FU) group and a 5-FU combined with CKI group to simulate the actual clinical combination drug use (Fig. 1A). Throughout treatment, subcutaneous tumor growth was faster in the vehicle group than in the other groups. After treatment, mice given CKI alone or 5-FU combined with CKI had a lower subcutaneous tumor volume, weight, and tumor burden (the ratio of subcutaneous tumor weight-to-body weight) than those in the vehicle group. The tumor burden in the 5-FU + CKI 130 mg kg^{-1} group was signi cantly lower than that in the 5-FU group. The body weight of mice in the 5-FU group was signi cantly lower than that of mice in the vehicle group. However, this phenomenon did not occur in mice in the 5-FU combined with CKI group (Fig. 1B and C). These results suggest that CKI intervention inhibits GC growth.

The subcutaneous tumor sections of the vehicle group showed tumorous tissue structures with interlaced cells arranged in a woven pattern, irregular shapes, varied sizes, nuclear ssion phases, high nuclear atypia, extruded cancer nests, necrosis, red blood cell in ltration, vascular proliferation, fat vacuoles, and in ammatory cell in ltration. Compared with those in the vehicle group, the degree of structural abnormalities in the tumor tissues in each treatment group was reduced. Some tumor cells showed balloon-like degeneration; there were fewer fat vacuoles; and there was less in ammatory cell in ltration. Specifically, in some regions of tumor tissues in each treatment group, tumor cells were sparse, with dark staining and degeneration of the cytoplasm, and there were also large areas of necrosis in the 5-FU + CKI 130 mg kg^{-1} group (Fig. 1D), suggesting that CKI has an intervention effect on GC, both alone and in combination with 5-FU. We further detected the tumor cell proliferation index (proliferating cell nuclear antigen positive ratio, PCNA positive ratio) and tumor cell apoptosis index (TUNEL positive rate) in tumor tissues. Compared with those in the vehicle group, the PCNA positive ratio in each treatment group decreased signi cantly, especially in the 5-FU group and the 5-FU + CKI 130 mg kg^{-1} group (Fig. 1E). Similarly, the TUNEL positive rate was signi cantly increased in each treatment group. Notably, the CKI 130 mg kg^{-1} group and 5-FU group had similar TUNEL positive rates (Fig. 1F). Furthermore, ow cytometry was used to measure T-cell levels

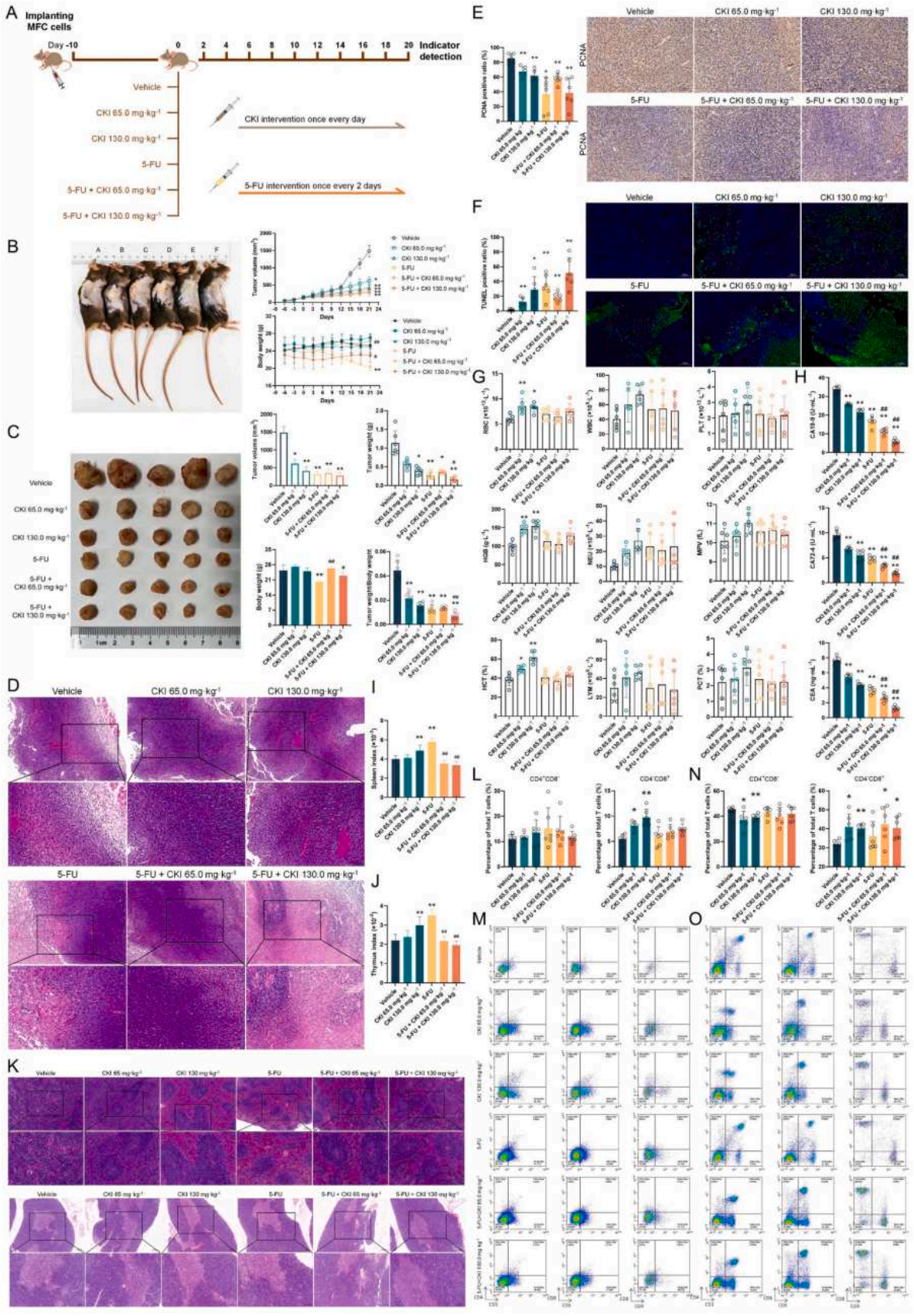

(caption on next page)

Fig. 1. CKI intervenes in multiple tumor pathophysiological indicators *in vivo* and enhances anti-GC effect of 5-FU. A) CKI *in vivo* intervention protocol based on the 615 strain mouse GC model. B) Mouse appearance and morphology (groups A-F represent the vehicle, 5-FU, CKI 65 mg kg^{-1}, CKI 130 mg kg^{-1}, 5-FU + CKI 65 mg kg^{-1}, and 5-FU + CKI 130 mg kg^{-1} groups, respectively), subcutaneous tumor volume monitoring and mouse body weight monitoring. C) Subcutaneous tumor tissue appearance and morphology (showing only ve representative tissues). Statistics are provided for subcutaneous tumor volume, subcutaneous tumor weight, mouse body weight, and the tumor weight-to-body weight ratio. D) H&E staining of subcutaneous tumor tissue sections. E) IHC staining of PCNA in subcutaneous tumor tissue sections. F) TUNEL staining of subcutaneous tumor tissue sections. G) Results of blood cell counts in mice. H) The levels of serum CA19–9, CA72–4 and CEA detected by ELISA. I) Spleen organ index. J) Thymus organ index. K) H&E staining of spleen (upper) and thymus (lower) tissue sections. L) Number of T cells in subcutaneous tumor tissue. M) Representative ow cytometry diagram of subcutaneous tumors. N) Number of T cells in the spleen. O) Representative ow cytometry diagram of the spleen. Statistical analyses were performed using unpaired Student's *t*-tests for comparisons between two groups and one-way ANOVA with Tukey's HSD post hoc tests for multi-group comparisons. The data are presented as *mean* ± *SD*, $n = 6$. Compared with the vehicle group, *: $P < 0.05$; **: $P < 0.01$· Compared with the 5-FU group, #: $P < 0.05$; ##: $P < 0.01$.

in tumor tissues. The CKI 65 mg kg^{-1} and CKI 130 mg kg^{-1} groups had signi cantly more $CD8^+$ T cells than the vehicle group. There was also an increase in $CD8^+$ T cells in the other treatment groups, but this increase was not statistically signi cant (Fig. 1L and M). The aforementioned results indicate that CKI has diverse pharmacological effects inhibiting the growth of GC tissue, inducing apoptosis in GC cells, and enhancing the in ltration of $CD8^+$ T cells into tumor tissues *in vivo*.

Blood samples showed that the number of red blood cells (RBC), hemoglobin concentration (HGB), and hematocrit (HCT) in the CKI 65 mg kg^{-1} group and CKI 130 mg kg^{-1} group were signi cantly greater than those in the vehicle group. The number of neutrophils (NEU) in the CKI 130 mg kg^{-1} group signi cantly increased. However, there was no signi cant difference in the quantitative blood indices, such as white blood cell (WBC) count, platelet count (PLT), or platelet speci c volume (PCT), between the groups (Fig. 1G). Notably, the concentrations of the GC blood markers CA19-9, CA72-4, and CEA were signi cantly reduced in all treatment groups, in a dose-dependent manner (Fig. 1H). Furthermore, the CKI 130 mg kg^{-1} group and the 5-FU combined with CKI group exhibited signi cantly greater spleen indices and thymus indices than those in the vehicle group (Fig. 1I and J). Additional H&E staining of spleen and thymus sections showed improvements in tissue structure and cell necrosis in all treatment groups compared with the vehicle group. The thymic capsule structure remained essentially intact without any noticeable thickening, and there was a decrease in the in ltration of in ammatory cells (Fig. 1K). Flow cytometry analysis revealed a signi cant decrease in the number of $CD4^+$ T cells in both the CKI 65 mg kg^{-1} group and the CKI 130 mg kg^{-1} group compared with that in the vehicle group. Moreover, with the exception of the 5-FU group, there was a signi cant increase in the quantity of $CD8^+$ T cells in every treatment group (Fig. 1N and O). The above results suggest that CKI may improve tolerance to subcutaneous tumors, inhibit the effects of blood markers, and regulate immune function in mice with GC.

3.3. CKI inhibits the proliferation, migration, invasion, and adhesion ability of GC cells in vitro

Using the SRB method, CKI intervention was applied to four human GC cell lines (AGS, HGC-27, MKN-45, and MKN-74) as well as a human normal gastric cell line (GES-1). The cell viability curves were plotted and the half-maximal inhibitory concentration (IC_{50}) values were calculated. After 24 h of CKI intervention, the HGC-27 cells had significantly lower IC_{50} values than the other GC cell groups. Similarly, after 48 h of intervention, both HGC-27 and MKN-45 cells had signi cantly lower IC_{50} values. After 72 h, there was no statistical difference in the IC_{50} values among the GC cell groups. Therefore, 48 h of sustained CKI intervention was determined to be the optimal experimental time condition (Fig. 2A and B). CKI increased the percentage of GC cells in G0&G1 phases but decreased the percentage of cells in the S phase. It also inhibited colony formation in AGS, HGC-27, and MKN-45 cells in a dose-dependent manner and reduced the EdU positive ratio (Fig. 2C–E). These results suggest that CKI can inhibit the proliferation of GC cells *in vitro* by inhibiting DNA replication and arresting the cell cycle. Transwell assays revealed a decrease in cell migration and invasion in the CKI intervention group compared with the control group (Fig. 2F–G). Cell adhesion experiments with Matrigel demonstrated that intervention with CKI resulted in a signi cant reduction in the number of GC cells that adhered to Matrigel (Fig. 2H).

3.4. Matching transcriptomic and proteomic results with CKI pharmacodynamic results

As shown in Fig. S2 and S3, after passing the quality inspection of RNA or protein samples to be tested, they were used for subsequent gene chip or TMT detection, respectively. At the transcriptional level, compared with the GES-1 group, the HGC-27 group of GC cells had 5441 differentially expressed mRNAs (DEmRNAs), 7840 differentially expressed lncRNAs (DElncRNAs), and 112 differentially expressed miRNAs (DEmiRNAs). Biological annotation and enrichment analysis showed that the DEmRNAs were mainly related to biological processes such as angiogenesis, cell adhesion, and positive regulation of cell migration, and were related to signaling pathways such as adhesion junction, TNF signaling pathway, Wnt signaling pathway, PI3K/AKT signaling pathway, and pathways in cancer. Compared with the GES-1 group, the MKN-45 group of GC cells had 5644 DEmRNAs, 6900 DElncRNAs, and 96 DEmiRNAs. Biological annotation and enrichment analysis revealed that the DEmRNAs were mainly related to biological processes such as cell migration, positive regulation of cell migration, and angiogenesis, and were related to signaling pathways such as TNF signaling pathway, TGF-β signaling pathway, gastric cancer pathway, Wnt signaling pathway, PI3K/AKT signaling pathway, and pathways in cancer. Compared with the HGC-27 group, the HGC-27+ CKI group had 2053 DEmRNAs, 5613 DElncRNAs, and 23 DEmiRNAs. Biological annotation and enrichment analysis showed that DEmRNAs were mainly related to biological processes such as angiogenesis, cell proliferation, and epithelial cell differentiation, and were related to signaling pathways such as DNA replication, intestinal immune network produced by IgA, chemical carcinogenesis-DNA adducts, and TGF-β signal pathway. Compared with the MKN-45 group, the MKN-45+ CKI group had 3696 DEmRNAs, 9251 DElncRNAs, and 58 DemiRNAs. Biological annotation and enrichment analysis showed that DEmRNAs were mainly related to biological processes such as cell proliferation regulation, angiogenesis, and cell migration, and were related to signaling pathways such as Hippo signaling pathway, ferroptosis, DNA replication, cell cycle, PI3K/AKT signaling pathway, and pathways in cancer.

At the protein level, compared with those in the GES-1 group, there were 2750 differentially expressed proteins (DEPs) in the HGC-27 group. Biological annotation and enrichment analysis showed that DEPs are related to biological processes such as cell cycle, leukocyte migration, and cytoskeletal network, and are related to signaling pathways such as DNA replication, tricarboxylic acid cycle, and ferroptosis. Compared with the GES-1 group, there were 2886 DEPs in the MKN-45 group. Biological annotation and enrichment analysis showed that DEPs are related to biological processes such as intercellular adhesion, cell migration, and cell cycle, and are related to signaling pathways such as ECM receptor interactions, Hippo signaling pathway, and oxidative phosphorylation pathway. Compared with the HGC-27 group, the HGC-27 + CKI group had 4476 DEPs. Biological annotation and enrichment

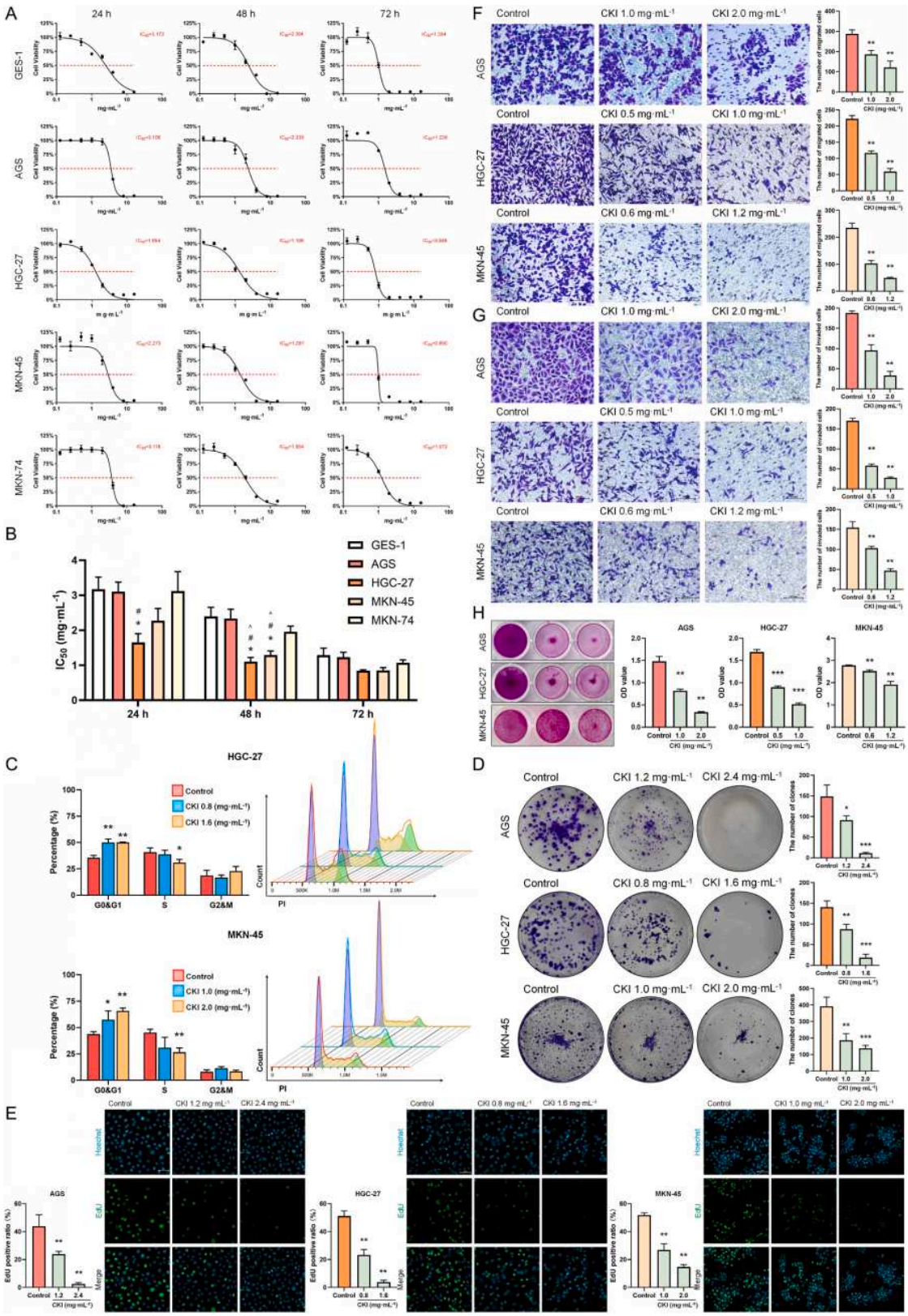

Fig. 2. CKI inhibits the proliferation, migration, invasion, and adhesion ability of GC cells *in vitro*. A) Cell viability curves after CKI intervention. B) Histogram of IC_{50} values for multiple cell types. Compared with the GES-1 group, *: $P < 0.05$; compared with the AGS group, $^{\#}$: $P < 0.05$; compared with the MKN-74 group, $^{\wedge}$: $P < 0.05$; $n = 3$. C–E) After GC cells were treated with various concentrations of CKI, the impact of CKI on the proliferation of GC cells, as determined by cell cycle distribution, colony formation ability, and EdU incorporation ability, was detected by ow cytometry, colony formation assay, and EdU incorporation assay, respectively. F–H) The effects of CKI on the migration, invasion, and adhesion of GC cells were assessed using Transwell assay. Statistical analyses were performed using unpaired Student's *t*-tests for comparisons between two groups and one-way ANOVA with Tukey's HSD post hoc tests for multi-group comparisons. The data are presented as *mean* ± *SD*. Compared with the control group, *: $P < 0.05$, **: $P < 0.01$, ***: $P < 0.001$, $n = 3$.

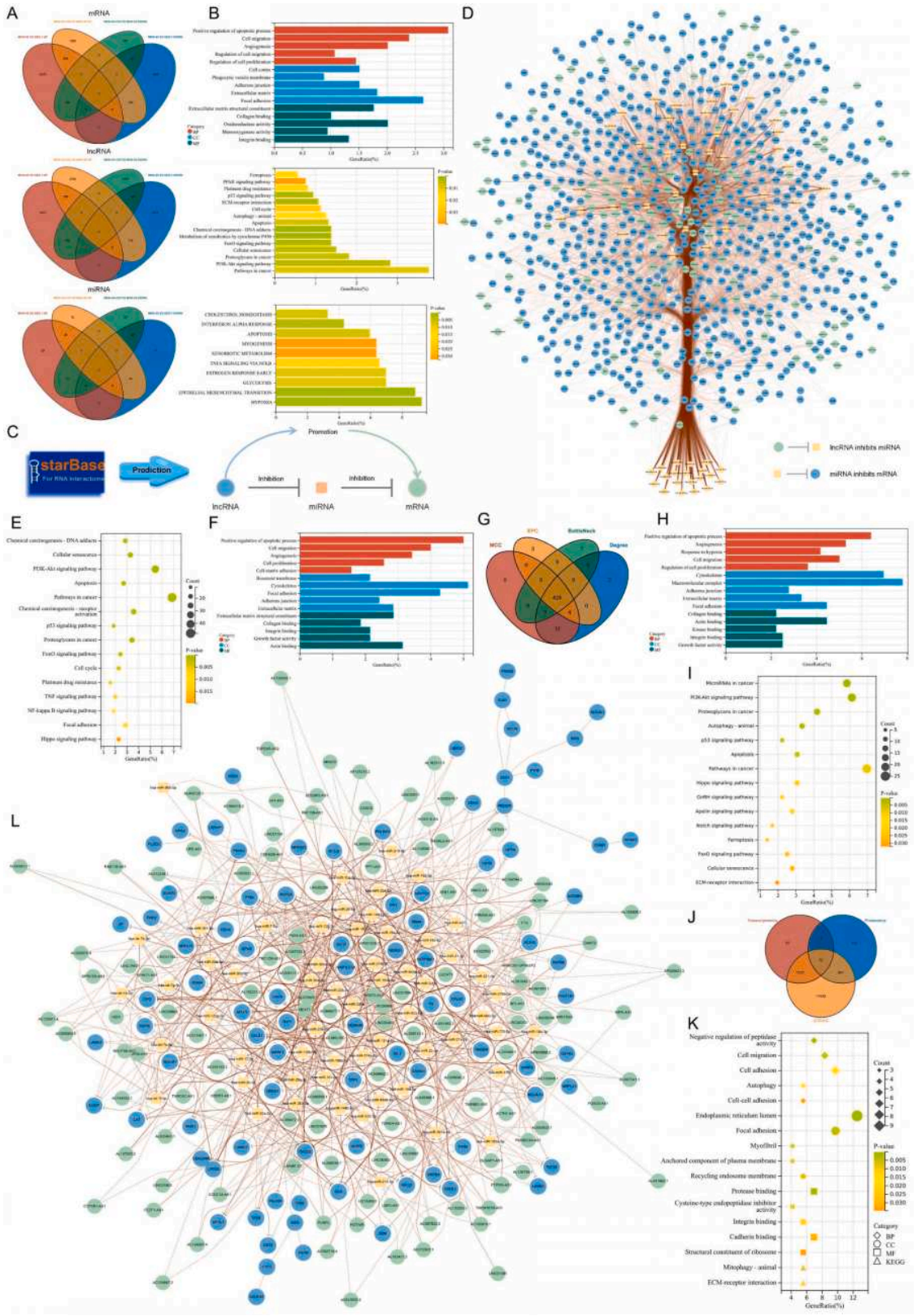

Fig. 3. The effect of CKI on the ceRNA network of GC cells. A-B) Venn diagram illustrating the pathways associated with aberrantly expressed genes affected by CKI intervention in GC cells and the results of mRNA enrichment analysis. C-D) Construction and visualization of CKI-GC ceRNA network I. E-F) Results of mRNA enrichment analysis of the CKI-GC ceRNA network I. G–I) Extraction of the modular sub-network shared by a total of four algorithms analyzed by BottleNeck, Degree, EPC, and MCC, and the results of mRNA enrichment analysis in this network. J–L) The intersection of transcriptomics results, proteomics results, and the human PPI network documented in the STRING database was used as an important node to extract the next sub-network from the aforementioned sub-network. This network was named CKI-GC ceRNA network II, and the results of the mRNA enrichment analysis of this network are shown.

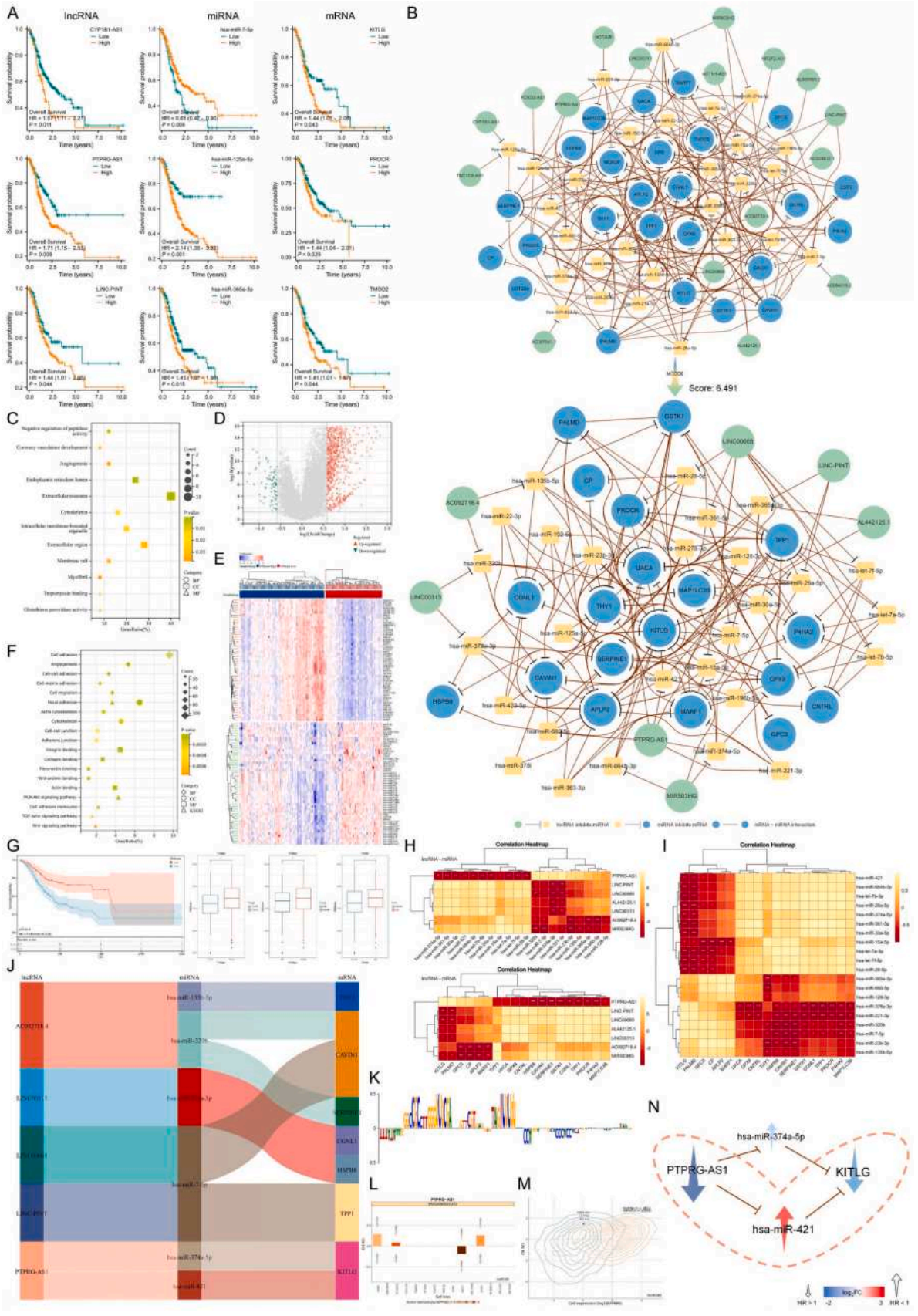

(caption on next page)

Fig. 4. PTPRG-AS1/hsa-miR-421/KITLG axis and its activated KITLG/KIT pathway are predicted to promote GC proliferation and metastasis. A) Kaplan-Meier curves for partial molecular survival analysis in CKI-GC ceRNA network II are presented. The results of the remaining molecular survival analyses are shown in Supplementary Fig. S7, S8, and S9. B-C) The molecules with survival signi cance in CKI-GC ceRNA network II were used as labeled nodes to extract sub-networks for CKI-GC ceRNA network III. After MCODE analysis, the resulting network was designated as the hub CKI-GC ceRNA network, and the results of the mRNA enrichment analysis were used to understand this network. D-G) Differentially expressed gene analysis, GO and KEGG enrichment analysis, and clinicopathological feature information of the CNScore High and CNScore Low groups. H-I) lncRNA, miRNA, and mRNA correlation analysis of the hub CKI-GC ceRNA network. J) Sankey diagram showing ceRNA axes consistent with ceRNA relationships. K-M) lncRNA subcellular localization prediction analysis. N) The PTPRG-AS1/hsa-miR-421/KITLG axis was predicted to be a potential key ceRNA axis.

Table 2
Relationship between CNScore and clinicopathologic factors among TCGA-STAD patients.

Characteristics	CNScore High ($n = 175$)	CNScore Low ($n = 117$)	Total ($n = 292$)	*P* value
Age				0.16
▉< 65	83 (28.42 %)	45 (15.41 %)	128 (43.84 %)	
▉111348 ≥ 65	92 (31.51 %)	72 (24.66 %)	164 (56.16 %)	
Gender				0.84
▉111348Female	64 (21.92 %)	45 (15.41 %)	109 (37.33 %)	
▉111348Male	111 (38.01 %)	72 (24.66 %)	183 (62.67 %)	
T stage				**6.60E−03**
▉111348T1	2 (0.68 %)	11 (3.77 %)	13 (4.45 %)	
▉T2	34 (11.64 %)	26 (8.90 %)	60 (20.55 %)	
▉T3	89 (30.48 %)	53 (18.15 %)	142 (48.63 %)	
▉T4	50 (17.12 %)	27 (9.25 %)	77 (26.37 %)	
N stage				**0.04**
▉N0	43 (14.73 %)	46 (15.75 %)	89 (30.48 %)	
▉N1	50 (17.12 %)	28 (9.59 %)	78 (26.71 %)	
▉N2	39 (13.36 %)	25 (8.56 %)	64 (21.92 %)	
▉N3	43 (14.73 %)	18 (6.16 %)	61 (20.89 %)	
M stage				0.96
▉M0	163 (55.82 %)	110 (37.67 %)	273 (93.49 %)	
▉M1	12 (4.11 %)	7 (2.40 %)	19 (6.51 %)	
Stage				**6.30E−04**
▉Stage I	11 (3.77 %)	26 (8.90 %)	37 (12.67 %)	
▉Stage II	58 (19.86 %)	38 (13.01 %)	96 (32.88 %)	
▉Stage III	87 (29.79 %)	42 (14.38 %)	129 (44.18 %)	
▉Stage IV	19 (6.51 %)	11 (3.77 %)	30 (10.27 %)	
Grade				0.19
▉G1	4 (1.37 %)	1 (0.34 %)	5 (1.71 %)	
▉G2	54 (18.49 %)	47 (16.10 %)	101 (34.59 %)	
▉G3	117 (40.07 %)	69 (23.63 %)	186 (63.70 %)	
Status				**2.20E−04**
▉Alive	88 (30.14 %)	85 (29.11 %)	173 (59.25 %)	
▉Dead	87 (29.79 %)	32 (10.96 %)	119 (40.75 %)	

analysis showed that the DEPs are related to biological processes such as cell cycle, apoptosis, and cell migration, and are related to signaling pathways such as DNA replication, adhesive bonding, and tight junctions. Compared with the MKN-45 group, the MKN-45 + CKI group had 1718 DEPs. Biological annotation and enrichment analysis showed that the DEPs are related to biological processes such as cell death regulation, cell-cell adhesion, and cell migration, and are related to signaling pathways such as nucleotide metabolism, lysosomes, and nucleocytoplasmic transport. In summary, the transcriptomic and proteomic results indicated that CKI was involved in multiple pathological and physiological pathways of GC, which was similar to the *in vitro* and *in vivo* pharmacological evaluation results.

3.5. Establishing the CNScore and its application: CKI-GC ceRNA network-mediated biological functions are associated with GC proliferation and metastasis

Identify genes that show differential expression before and after CKI treatment in GC cells, compare them with genes that are differentially expressed between GC and GES-1 cells, and use the overlapping genes as the regulatory gene set for CKI in GC cells, representing the abnormally expressed genes of CKI intervening in GC. The abnormally expressed CKI genes in MKN-45 cells were enriched in biological processes such as positive regulation of cell apoptosis, cell migration, and angiogenesis; in cell components such as cell cortex, adhesive junctions, and focal adhesions; in molecular functions such as extracellular matrix structural components, oxidoreductase activity, and integrin binding; in signaling pathways such as protein glycans in cancer, PI3K/AKT signaling pathways, and cancer pathogenesis pathways; and in biological functional items such as hypoxia, epithelial mesenchymal transition, and glycolysis (Fig. 3A-B). The relationships of ceRNA with lncRNAs, miRNAs, and mRNAs were predicted using the starBase database, and the CKI-GC ceRNA network I (880 nodes, 8368 edges) was constructed. The mRNAs in this network were enriched in biological processes such as positive regulation of cell apoptosis, cell migration, and angiogenesis; in cellular components such as cytoskeleton, focal adhesion, and extracellular matrix; in molecular functions such as actin binding, extracellular matrix structural components, and growth factor activity; and in signaling pathways such as the pathogenesis of cancer, PI3K/AKT signaling pathway, and cell cycle (Fig. 3C–E). The intersection of the sub-networks of the 4 modules was enriched in biological processes such as forward regulation of apoptosis, angiogenesis, and cell migration; and in signaling pathways such as pathways in cancers, microRNAs in tumors, and PI3K/AKT signaling pathways (Fig. 3G-I and Fig. S4D-G). The intersection of the transcriptomics results, proteomics results, and PPI network in the STRING database with human genes was used to construct CKI-GC ceRNA network II (271 nodes, 1384 edges). The mRNAs in this network were enriched in biological processes such as negative regulation of peptidase activity, cell migration, and cell adhesion; and in signaling pathways such as mitochondrial phagocytosis and

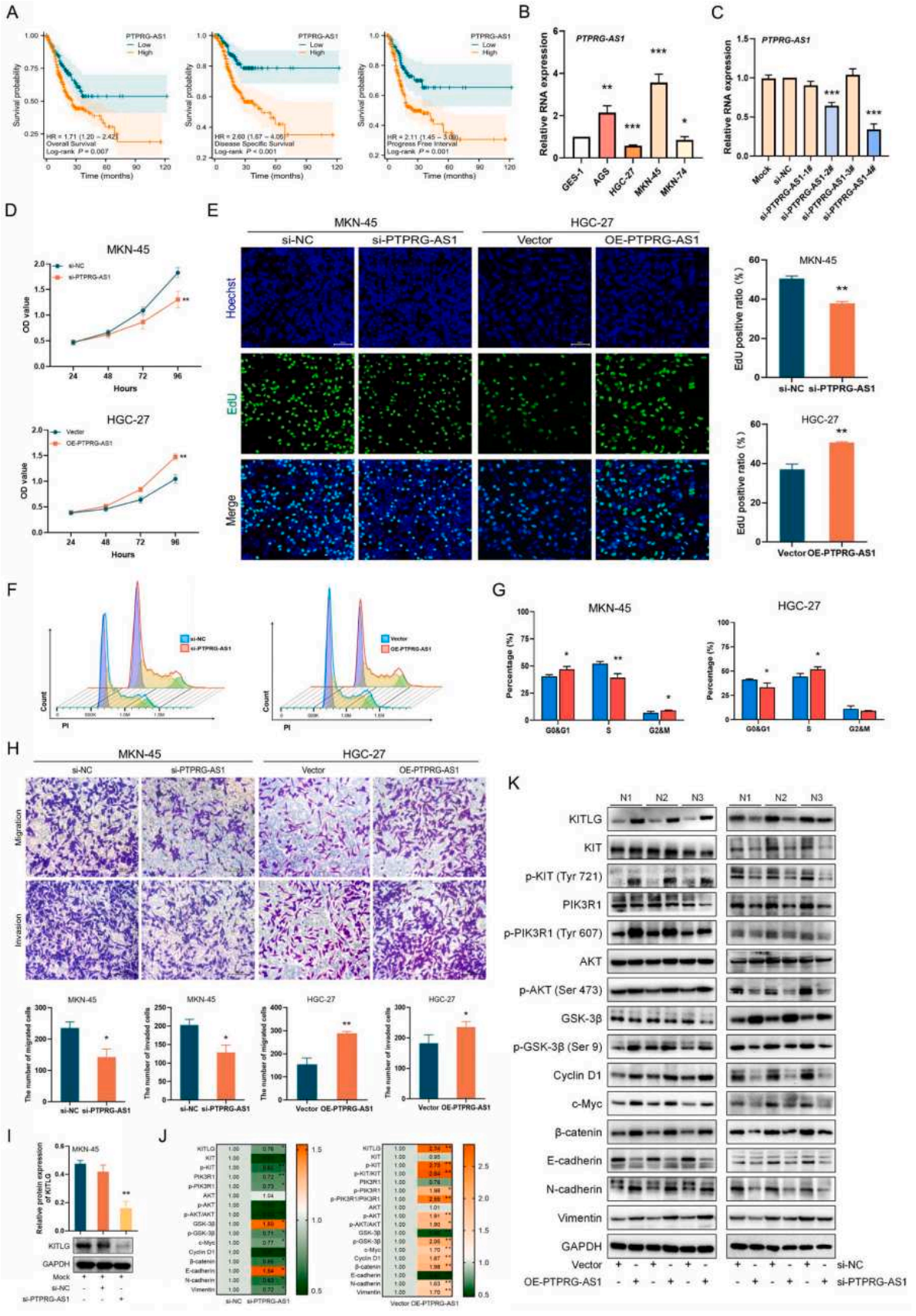

(caption on next page)

Fig. 5. PTPRG-AS1 promotes the proliferation, migration, and invasion of GC cells by upregulating KITLG/KIT pathway. A) Survival analysis of TCGA-based GC patients strati ed according to PTPRG-AS1 expression. B) Relative expression of PTPRG-AS1 in various GC cell lines normalized to that in GES-1 cells. C) Relative expression of PTPRG-AS1 after transient transfection with different PTPRG-AS1 siRNAs. D-G) CCK-8 assay, EdU incorporation assay, and ow cytometry were used to assess the proliferation of MKN-45 cells transiently transfected with si-PTPRG-AS1 or si-NC or HGC-27 cells transiently transfected with OE-PTPRG-AS1 or vector. This included assessing cell viability, EdU incorporation capacity, and the cell cycle. Scale bar = 50 μm. H) Transwell assays were used to assess the cell migration and invasion ability of MKN-45 cells transiently transfected with si-PTPRG-AS1 or si-NC or HGC-27 cells transiently transfected with OE-PTPRG-AS1 or vector. Scale bar = 100 μm. I-K) Relative expression of KITLG proteins and KITLG/KIT pathway-associated proteins was detected by Western blot in MKN-45 cells transiently transfected with si-PTPRG-AS1 or si-NC or HGC-27 cells transiently transfected with OE-PTPRG-AS1 or vector. Statistical analyses were performed using unpaired Student's *t*-tests for comparisons between two groups and one-way ANOVA with Tukey's HSD post hoc tests for multi-group comparisons. The data are presented as *mean* ± *SD*. Compared with the si-NC group (or the vector group), *: $P < 0.05$, **: $P < 0.01$, ***: $P < 0.001$, $n = 3$.

ECM receptor interactions (Fig. 3J–L). As shown in Fig. 4A-B and Fig. S7A, S8A and S9A, the clinical prognostic information of GC patients (TCGA-STAD) was introduced into CKI-GC ceRNA network II. After the genes with prognostic signi cance were retained, the CKI-GC ceRNA network III (70 nodes, 308 edges) was constructed. The MCODE algorithm extracted the sub-network of the main module and constructed the hub CKI-GC ceRNA network (54 nodes, 217 edges). The analysis of the ceRNA network of CKI in HGC-27 cells was consistent with that in MKN-45 cells mentioned above (Fig. S5, S6, S7B, S8B and S9B). Due to the absence of lncRNAs in the hub ceRNA network of HGC-27 cells, the ceRNA ternary lncRNA-miRNA-mRNA relationship was lost. Therefore, subsequent research will focus on CKI intervention in the hub ceRNA network of MKN-45 GC cells. The mRNAs in the hub CKI-GC ceRNA network are mainly enriched in biological processes such as negative regulation of peptidase activity, coronary vascular system development, and angiogenesis (Fig. 4C). The results indicate that, as the network shrinks, fewer mRNAs are used for enrichment analysis, and the results of the enrichment analysis become more limited.

As shown in Fig. 4D–F and Fig. S4H, the CNScore was used to rate the hub CKI-GC ceRNA network, and the CNScore High group and CNScore Low group were divided based on the optimal cutoff point. The differences in parameters between the CNScore High and CNScore Low groups represent the biological and clinical signi cance of the hub CKI-GC ceRNA network in GC. Compared with those in the CNScore Low group, the DEGs in the CNScore High group were related to biological processes such as cell adhesion, angiogenesis, and cell migration; cellular components such as focal adhesion, actin cytoskeleton, and cytoskeleton; molecular functions such as integrin binding, collagen binding, and bronectin binding; signaling pathways such as focal adhesion, PI3K/AKT signaling pathway, and cell adhesion molecules; and biological functional gene set entries such as PI3K/AKT/MTOR signaling, TGF-β Signal, epithelial mesenchymal transition, Wnt/β-catenin signaling, Notch signaling, and neovascularization. Biological manifestations of GC in the CNScore High group tend to be related to tumor metastasis, tumor metabolism, and tumor differentiation, while those in the CNScore Low group tend to be related to tumor growth and proliferation. Compared with the CNScore Low group, the CNScore High group has a lower likelihood of survival (*HR* = 2.18, 95 % *CI*: 1.45–3.28, $P = 1.2E\text{-}4$). The CNScore was positively correlated with the T stage, N stage, and G grade of GC (Fig. 4G and Fig. S4I). T stage, N stage, clinical stage, and survival status were signi cantly associated with the CNScore (Table 2). These results suggest that the biological signi cance of the hub CKI-GC ceRNA network annotated by the CNScore may lie in the growth, migration, invasion, and other aspects of GC, while the clinical signi cance may lie in the risk of metastasis and the prediction of the survival probability of GC patients.

3.6. The PTPRG-AS1/hsa-miR-421/KITLG axis and its activation of the KITLG/KIT pathway were predicted to be an important mechanism promoting GC proliferation and metastasis

As shown in Fig. 4J–N and Fig. S4J–L, after analyzing the correlation between different molecules and predicting the subcellular localization of lncRNAs, it was found that the PTPRG-AS1/hsa-miR-374a-5p/KITLG axis and PTPRG-AS1/hsa-miR-421/KITLG axis in the hub CKI-GC ceRNA network had a greater likelihood of real existence. Considering the gene expression pro les of MKN-45 and HGC-27 cells, CKI downregulated the expression of PTPRG-AS1 (*HR* = 1.71, 95 % *CI*: 1.15–2.53) and KITLG (*HR* = 1.44, 95 % *CI*: 1.01–2.06), downregulated the expression of hsa-miR-374a-5p (*HR* = 0.68, 95 % *CI*: 0.49–0.93), and upregulated the expression of hsa-miR-421 (*HR* = 0.66, 95 % *CI*: 0.48–0.89). Therefore, the PTPRG-AS1/hsa-miR-421/KITLG axis was ultimately identi ed as the key ceRNA axis of the hub CKI-GC ceRNA network, de ned as "Key ceRNA axis of CKI intervention in GC". Due to the unclear function and mechanism of action of PTPRG-AS1 in GC, bioinformatics analysis related to GC was conducted on PTPRG-AS1. The results showed that high expression of PTPRG-AS1 predicted higher T stage, poorer prognosis, and greater activation of signaling pathways that related to the growth, proliferation, and metastasis of GC, such as TNFα signal activated by NFκB, Wnt/β-catenin signal, Notch signal, EMT, and angiogenesis (Fig. S10 and Table S2). Taken together, the CNScore predicted that the CKI-GC core ceRNA network is involved in promoting growth, proliferation, and metastasis of GC through pathways such as cell adhesion, cell movement, PI3K/AKT, and Wnt signaling. Moreover, KITLG binds to its unique receptor KIT and activates the KITLG/KIT pathway, leading to various biological effects. Based on the results mentioned above, considering the main involvement of KITLG in pathways in cancer (KEGG map05200) and PI3K/AKT signaling pathways (KEGG map04151), it is speculated that the PTPRG-AS1/hsa-miR-421/KITLG axis regulates the growth, proliferation, and metastasis phenotype of GC mediated by downstream PI3K/AKT/GSK-3β/c-Myc, PI3K/AKT/GSK-3β/CCND1, and PI3K/AKT/GSK-3β/β-catenin by activating the KITLG/KIT signaling pathway. Moreover, E-cadherin, N-cadherin, and Vimentin, which are considered as EMT markers and downstream target proteins of β-catenin, are designed as potential indicators of GC metastasis.

3.7. PTPRG-AS1 promotes the proliferation, migration, and invasion of GC cells by upregulating the KITLG/KIT pathway

High PTPRG-AS1 expression can signi cantly predict a poor prognosis in GC patients in terms of overall survival (OS), disease-speci c survival (DSS), and progression free interval (PFI), as shown in Fig. 5A. Fig. 5B shows PTPRG-AS1 expression in the GC cell lines AGS, HGC-27, MKN-45, and MKN-74 normalized to that in GES-1 cells. MKN-45 had the highest, while HGC-27 had the lowest expression. Therefore, PTPRG-AS1 knockdown and overexpression experiments were conducted using MKN-45 and HGC-27 cell lines. To effectively knock down PTPRG-AS1, we designed 4 siRNAs for experimentation. The results showed that si-PTPRG-AS1-2# and si-PTPRG-AS1-4# signi cantly reduced the RNA expression of PTPRG-AS1 (Fig. 5C), therefore si-PTPRG-AS1-4#, which exhibited increased knockdown ef ciency was selected for subsequent experiments. Compared with those in the si-NC group, the optical density (OD) of the si-PTPRG-AS1 group was signi - cantly lower; the EdU positive ratio signi cantly decreased; the proportion of G0&G1 phase signi cantly increased, while the proportion of S phase signi cantly decreased. The number of cells that migrated and invaded through the Transwell membrane was signi cantly lower (Fig. 5D–H). In contrast, compared with those in the vector group, there were signi cant increases in the OD, EdU positive ratio, proportion of

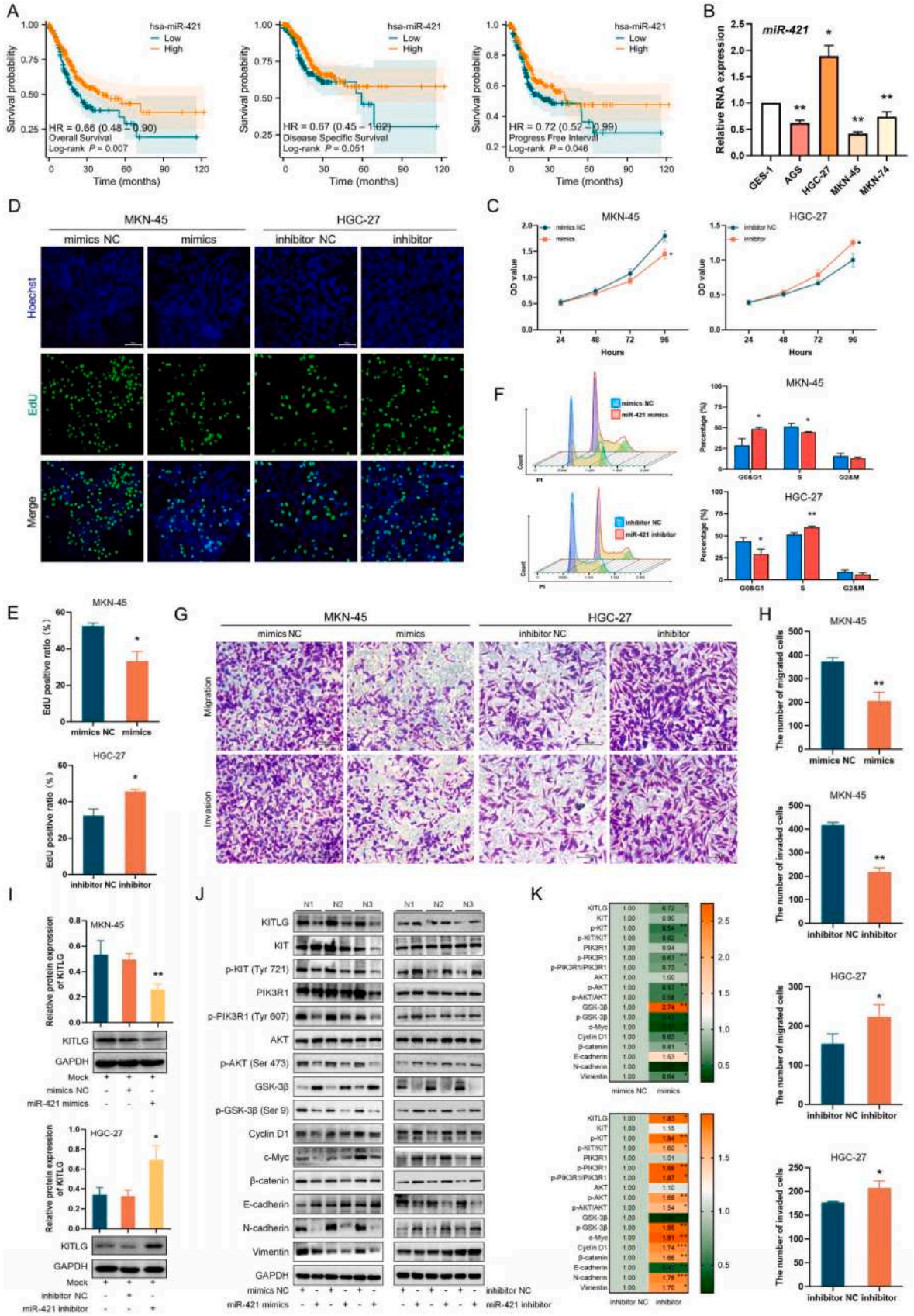

(caption on next page)

Fig. 6. Hsa-miR-421 inhibits proliferation, migration, and invasion of GC by targeting KITLG and downregulating KITLG/KIT pathway. A) Survival analysis of patients strati ed by overall survival, disease-speci c survival, and progression-free interval according to hsa-miR-421 expression. B) The relative expression of hsa-miR-421 in various GC cell lines after normalization to that in GES-1 cells. C-F) Following the transient transfection of hsa-miR-421 mimics and hsa-miR-421 inhibitor into MKN-45 cells and HGC-27 cells, the effects of the mimics and inhibitor on the proliferation capacity of GC cells, including cell viability, EdU incorporation ability, and cell cycle, were assessed using the CCK-8 assay, EdU incorporation assay, and ow cytometry, respectively. Scale bar = 50 μm. G and H) Cell migratory and invasive capabilities were evaluated using Transwell assays with MKN45 cells transfected with mimics or mimics NC and HGC-27 cells transfected with inhibitor or inhibitor NC. Scale bar = 100 μm. I-L) The relative expression of KITLG protein and KITLG/KIT pathway-associated proteins was detected using Western blotting after transient transfection of MKN-45 cells and HGC-27 cells with hsa-miR-421 mimics and inhibitor, respectively. Statistical analyses were performed using unpaired Student's *t*-tests for comparisons between two groups and one-way ANOVA with Tukey's HSD post hoc tests for multi-group comparisons. The data are presented as *mean* ± *SD*. Compared with the NC group, *: $P < 0.05$, **: $P < 0.01$, ***: $P < 0.001$, $n = 3$.

cells in S phase proportion, and cell migration and invasion in the OE-PTPRG-AS1 group. Subsequent investigation revealed that knocking down PTPRG-AS1 led to a decrease in KITLG protein expression and changes in downstream proteins related to the KITLG/KIT pathway. Speci cally, the protein expression levels of KIT, p-GSK-3β, β-catenin, c-Myc, and Cyclin D1 decreased, the protein phosphorylation ratios of PIK3R1 and AKT decreased, and the protein expression level of GSK-3β increased. In contrast, compared with the PTPRG-AS1 knockdown, PTPRG-AS1 overexpression resulted in the opposite phenomenon compared to knocking down PTPRG-AS1 effects (Fig. 5I–K). The above results indicate that PTPRG-AS1 is a gene that promotes GC malignant growth, proliferation, and metastasis. Knocking down KITLG inhibits malignant progression and reduces KITLG/KIT pathway activity.

3.8. Hsa-miR-421 downregulates the KITLG/KIT pathway by targeting KITLG, thereby inhibiting the proliferation, migration, and invasion ability of GC cells

Low expression of hsa-miR-421 signi cantly predicts a poor prognosis in GC patients in terms of OS and PFI (Fig. 6A). Fig. 6B shows the expression of hsa-miR-421 relative to GES-1 in AGS, HGC-27, MKN-45, and MKN-74 cells, with MKN-45 and HGC-27 exhibiting the lowest and highest expression of hsa-miR-421, respectively. Therefore, subsequent hsa-miR-421 overexpression and knockdown experiments were conducted using MKN-45 and HGC-27 cell lines. Compared with the mimics NC group, the hsa-miR-421 mimics group showed signi cantly reduced OD values, a decreased EdU positive ratio, an increased proportion of cells in the G0&G1 phase, a decreased proportion of cells in the S phase, and decreased migration and invasion through the Transwell membrane compared with the mimics NC group. Conversely, compared with those in the inhibitor NC group, the OD value, EdU positive ratio, S phase proportion, and the number of migrating and invading cells in the hsa-miR-421 inhibitor group were signi cantly increased, while there was a signi cant decrease in the number of cells in the G0&G1 phase (Fig. 6C–H). Further research found that after transfection with hsa-miR-421 mimics, the protein expression level of KITLG decreased, and the expression of downstream proteins related to the KITLG/KIT pathway changed. Moreover, the protein expression levels of p-GSK-3β, β-catenin, c-Myc, and Cyclin D1 decreased; the protein phosphorylation ratios of KIT, PIK3R1, and AKT decreased; and the protein expression level of GSK-3β increased. In contrast, transfection of hsa-miR-421 inhibitor had the opposite effects as transfection of hsa-miR-421 mimics (Fig. 6I–K). Overall, high expression of hsa-miR-421 inhibits the malignant growth, proliferation, and metastasis of GC, and reduces the activity of the KITLG/KIT pathway. On the other hand, inhibiting hsa-miR-421 promotes malignant progression of GC and increases the activity of the KITLG/KIT pathway.

3.9. PTPRG-AS1 releases KITLG through sponge adsorption of hsa-miR-421, thereby upregulating the KITLG/KIT pathway to promote the proliferation, migration, and invasion of GC cells

Subcellular localization of lncRNAs, dual luciferase reporter gene assay, and rescue assays were used to verify whether the relationship of the ceRNA and PTPRG-AS1/hsa-miR-421/KITLG axis existed in GC cells. The results of the nucleocytoplasmic separation showed that PTPRG-AS1 was distributed in both the cytoplasm and nucleus, which was consistent with the conditions of the ceRNA mechanism (Fig. 7A). Similar to the approach used for studying PTPRG-AS1, we selected MKN-45 and HGC-27 cells for subsequent KITLG knockdown and overexpression experiments, and used si-KITLG-1# with higher knockdown ef ciency for transient knockdown of KITLG (Fig. 7B-C). After the knockdown of PTPRG-AS1, the RNA expression of KITLG decreased, and the RNA expression of hsa-miR-421 increased. However, the overexpression of PTPRG-AS1 led to the opposite results (Fig. 7D). Furthermore, to con rm the results of the bioinformatics prediction analysis, PTPRG-AS1-WT and PTPRG-AS1-MUT were cloned and inserted into luciferase reporter vector pSI-Check2. Dual luciferase reporter assay showed that, compared with that in the hsa-miR-421 mimics NC group, the activity of the luciferase reporter vector containing the PTPRG-AS1-WT sequence decreased signi cantly in the hsa-miR-421 mimics group. However, it was signi cantly greater in the hsa-miR-421 inhibitor group than in the hsa-miR-421 inhibitor NC group. However, these phenomena were not detected for the mutated PTPRG-AS1 binding sites. These ndings suggested that PTPRG-AS1 directly binds to hsa-miR-421 in GC cells. Similarly, to con rm the direct interaction between KITLG and hsa-miR-421, KITLG-3' UTR-WT and KITLG-3' UTR-MUT were inserted into the luciferase reporter vector pSI-Check2. The results demonstrated that, compared with that in the hsa-miR-421 mimics NC group, the activity of the luciferase reporter vector carrying the KITLG-3' UTR-WT sequence was signi cantly lower in the hsa-miR-421 mimics group. However, it was signi cantly greater in the hsa-miR-421 inhibitor group than in the hsa-miR-421 inhibitor NC group. Nevertheless, there was no difference in the luciferase activity among the hsa-miR-421 mimics, mimics NC, hsa-miR-421 inhibitor, and inhibitor NC groups in the KITLG-3' UTR-MUT group (Fig. 7E). The above results indicated that there was a direct binding between KITLG and hsa-miR-421 in GC cells. As shown in Fig. 7F–O, compared with those in the sh-NC group, the OD, EdU positive ratio, and proportion of cells in S phase in the sh-PTPRG-AS1 group were signi cantly lower, while the proportion of cells in G0&G1 phase was signi cantly greater. The number of cells that migrated and invaded through the Transwell membrane signi cantly decreased. The above changes were accompanied by a decrease in the RNA expression level of KITLG; a decrease in the protein expression levels of KITLG, KIT, p-GSK-3β, β-catenin, c-Myc, and Cyclin D1; a decrease in the protein phosphorylation ratios of PIK3R1 and AKT; and a decrease in the protein expression level of GSK-3β. These results indicate a decrease in the activity of the KITLG/KIT pathway, as well as changes in the protein expression levels of growth-, proliferation-, and metastasis-related indicators in GC. Hsa-miR-421 inhibition rescues the inhibition of the malignant phenotype of GC caused by PTPRG-AS1 knockdown, increasing the expression level of KITLG and restoring the activity of the KITLG/KIT pathway. There were also changes in protein indicators related to the growth, proliferation, and metastasis of GC. Similarly, hsa-miR-421 mimics weaken the enhanced malignant phenotype of GC caused by the overexpression of PTPRG-AS1, decrease the expression level of KITLG, inhibit the activity of the KITLG/KIT pathway, and alter the protein expression levels of growth, proliferation, and metastasis related indicators in GC.

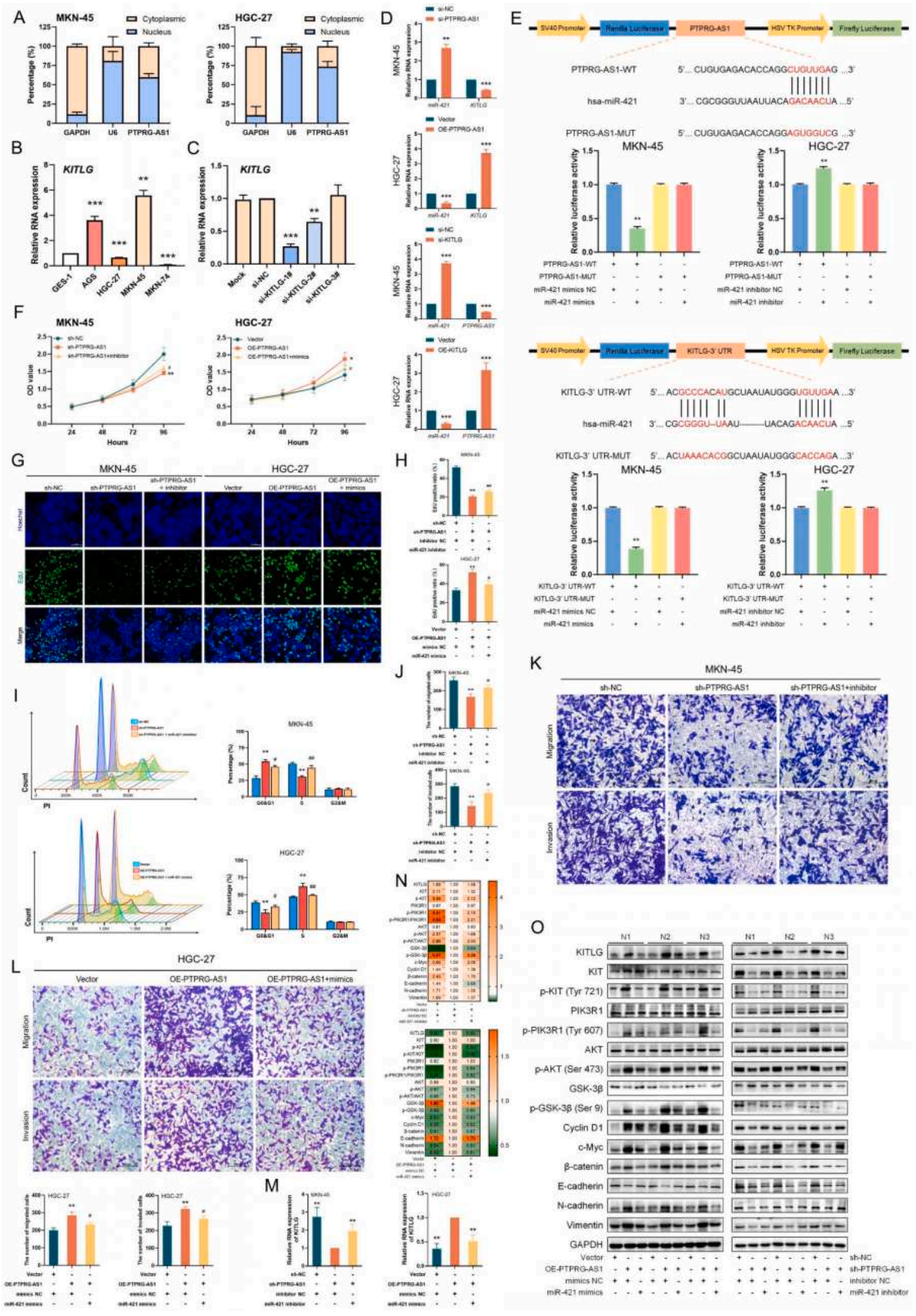

(caption on next page)

Fig. 7. PTPRG-AS1 sponges hsa-miR-421, releases KITLG, and upregulates KITLG/KIT pathway, promoting the malignant behavior of GC. A) Subcellular localization of PTPRG-AS1 in GC cells detected by nucleoplasmic separation. B) Relative expression of KITLG in various GC cell lines normalized to that in GES-1 cells. C) Relative expression of KITLG after transient transfection with different KITLG siRNAs. D) The relative expression of the other RNAs in the ceRNA axis determined by RT-qPCR after transient knockdown or overexpression of PTPRG-AS1 or KITLG. E) Dual-luciferase reporter gene assay to validate the MRE binding ability between PTPRG-AS1 and hsa-miR-421, or KITLG and hsa-miR-421. F-I) The CCK-8 assay, EdU incorporation assay, and ow cytometry were used to assess the effects of the hsa-miR-421 inhibitor or mimics on the proliferation of MKN-45 cells stably transfected with sh-PTPRG-AS1 or sh-NC or HGC-27 cells stably transfected with OE-PTPRG-AS1 or vector. Scale bar = 50 μm. J–L) Transwell assays were used to assess the effects of hsa-miR-421 inhibitor or mimics on the cell migration and invasion ability of MKN-45 cells stably transfected with sh-PTPRG-AS1 or sh-NC or HGC-27 cells stably transfected with OE-PTPRG-AS1 or vector. Scale bar = 100 μm. M-O) RT-qPCR and Western blotting were used to detect the effects of the hsa-miR-421 inhibitor or mimics on the relative expression of RNA or protein of KITLG and KITLG/KIT pathway-associated proteins in MKN-45 cells stably transfected with sh-PTPRG-AS1 or sh-NC or HGC-27 cells stably transfected with OE-PTPRG-AS1 or vector. Statistical analyses were performed using unpaired Student's *t*-tests for comparisons between two groups and one-way ANOVA with Tukey's HSD post hoc tests for multi-group comparisons. The data are presented as *mean* ± *SD*. Compared with the sh-NC group (or vector group), *: $P < 0.05$, **: $P < 0.01$, ***: $P < 0.001$. Compared with the sh-PTPRG-AS1 group (or OE-PTPRG-AS1 group), #: $P < 0.05$, ##: $P < 0.01$, $n = 3$.

3.10. Knockdown of PTPRG-AS1 inhibits GC growth and metastasis in vivo, whereas overexpression of PTPRG-AS1 resulted in the opposite effects

To further investigate the effects of the PTPRG-AS1/hsa-miR-421/KITLG axis *in vivo*, stable knockdown of PTPRG-AS1 and stable overexpression of PTPRG-AS1 in MKN-45 and HGC-27 cells were used to construct mouse liver metastasis models of GC. MRI revealed that compared with the sh-NC group, the sh-PTPRG-AS1 group had signi cantly smaller areas and fewer cancer nests with GC liver metastasis. The liver appearance and H&E staining results were consistent with the MRI results. IHC results showed that knocking down PTPRG-AS1 led to a decrease in the protein expression levels of KITLG and PCNA in the liver metastasis nests of GC. In addition, the concentration of KITLG in mouse serum signi cantly decreased (Fig. 8A–F). MRI revealed that, compared with the vector group, the OE-PTPRG-AS1 group had larger areas and more cancer nests with GC liver metastasis. Consistent results were observed for liver appearance and H&E staining. The overexpression of PTPRG-AS1 led to increased protein expression of KITLG and PCNA in the liver metastasis nests of GC, as shown by the IHC results. Furthermore, the concentration of KITLG in mouse serum signi cantly increased (Fig. 8G–L). The presence of cancer nest tissue in GC liver metastases was further detected via RT-qPCR and Western blot analysis, and the results revealed that the expression of PTPRG-AS1 was positively correlated with that of KITLG and negatively correlated with that of hsa-miR-421. Compared with those in the sh-NC group, the protein expression levels of KITLG, p-GSK-3β, c-Myc, and Cyclin D1 in the sh-PTPRG-AS1 group were signi cantly lower; the protein phosphorylation ratios of KIT, PIK3R1, and AKT were decreased; and the protein expression level of GSK-3β was signi cantly increased, which indicated a decrease in the activity of the KITLG/KIT pathway. In contrast, overexpression of PTPRG-AS1 led to the opposite results, indicating an enhanced activity of the KITLG/KIT pathway (Fig. 8M–O). The results of the *in vivo* experiments were consistent with those of the *in vitro* experiments, indicating the existence of the PTPRG-AS1/hsa-miR-421/KITLG axis and its biological effects in GC.

3.11. CKI downregulates the KITLG/KIT pathway by regulating the PTPRG-AS1/hsa-miR-421/KITLG axis, thereby inhibiting the proliferation, migration, and invasion ability of GC cells

We validated the regulatory effect of CKI on the PTPRG-AS1/hsa-miR-421/KITLG axis in an *in vitro* GC cell model. The results showed that CKI can inhibit the RNA expression of PTPRG-AS1 and KITLG in MKN-45 and HGC-27 cells; promote the RNA expression of hsa-miR-421; regulate the expression of growth-, proliferation-, and metastasis-related proteins downstream of the KITLG/KIT pathway in GC; and inhibit the activity of the KITLG/KIT pathway and the malignant progression of GC. In addition, similar results were found in the subcutaneous tumor tissue of GC in the *in vivo* experiments (Fig. 9A-B and Fig. S11). Similar to the results of the PTPRG-AS1 rescue experiment, overexpression of PTPRG-AS1 or inhibition of hsa-miR-421 rescued the inhibitory effect of CKI on the malignant phenotype of GC cells, with an increase in RNA expression of KITLG, recovery of KITLG/KIT pathway activity, and changes in marker proteins related to malignant growth, proliferation, and metastasis of GC (Fig. 9C–I). These results indicate that CKI inhibits the growth, proliferation, migration, and invasion ability of GC cells *in vitro* by targeting the PTPRG-AS1/hsa-miR-421/KITLG axis and inhibiting the KITLG/KIT signaling pathway.

3.12. CKI downregulates the KITLG/KIT pathway by regulating the PTPRG-AS1/hsa-miR-421/KITLG axis, thereby inhibiting the growth, proliferation, and metastasis of GC

Then, we validated the regulatory effect of CKI on the PTPRG-AS1/hsa-miR-421/KITLG axis in a mouse model of GC liver metastasis. The MRI ndings indicated that the CKI 65.0 mg kg^{-1} and CKI 130.0 mg kg^{-1} groups exhibited signi cantly reduced areas and fewer cancer nests of GC liver metastases than the vehicle group. Consistent results were observed in the evaluation of the liver appearance and H&E staining. IHC analysis revealed decreased protein expression levels of KITLG and PCNA in liver metastasis nests of GC following CKI intervention, accompanied by a signi cant decrease in the KITLG concentration in the mouse serum (Fig. 10A–F). RT—qPCR and Western blotting were performed on cancerous GC nest tissue from liver metastases. After CKI intervention, the RNA expression levels of PTPRG-AS1 and KITLG decreased, while the RNA expression level of hsa-miR-421 increased (Fig. 10G–I). Compared with those in the vehicle group, the protein expression levels of KITLG, KIT, p-GSK-3β, c-Myc, and Cyclin D1 in the CKI 65.0 mg kg^{-1} and CKI 130.0 mg kg^{-1} groups were signi cantly lower. The protein phosphorylation ratios of PIK3R1 and AKT decreased, and the protein expression level of GSK-3β signi cantly increased. These results indicated a decrease in the activity of the KITLG/KIT pathway.

Taken together, these ndings suggest that the lncRNA PTPRG-AS1 acts as a sponge for hsa-miR-421, releases KITLG, and upregulates the KITLG/KIT pathway to promote malignant growth, proliferation, and metastasis of GC. CKI inhibits the malignant progression of GC by regulating the PTPRG-AS1/hsa-miR-421/KITLG axis (Fig. 10J).

4. Discussion

The malignancy of GC is evident by the robust proliferation capabilities of GC cells [2,43]. Speci cally, it is manifested in uncontrolled cell cycle regulation, malignant invasive proliferation, strong survival

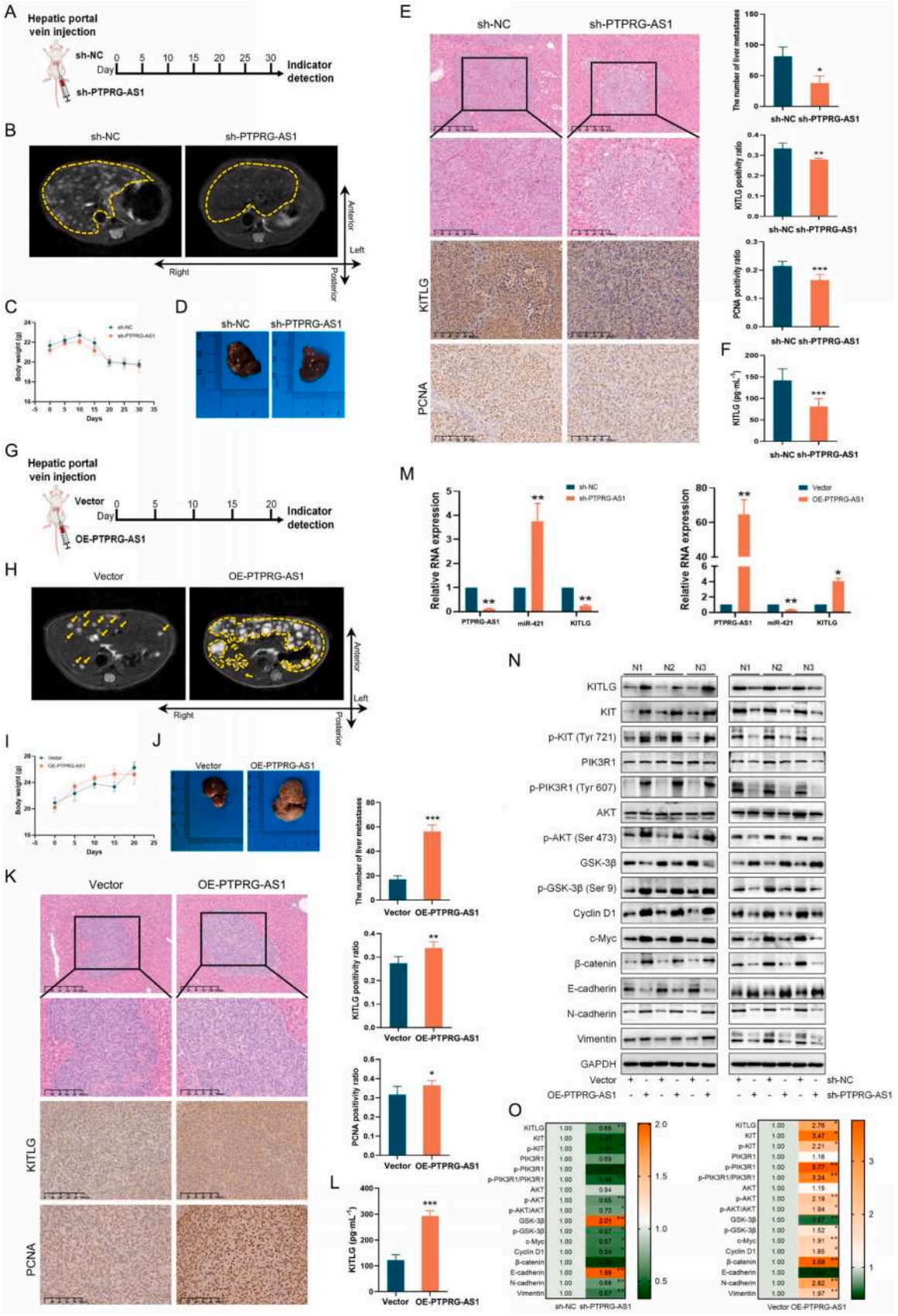

(caption on next page)

Fig. 8. Knockdown and overexpression of PTPRG-AS1 affects the growth and metastasis of GC *in vivo*. A) Schematic diagram of the experimental protocol showing the effect of PTPRG-AS1 knockdown on GC liver metastasis. B) MRI monitoring of GC liver metastasis. C) Body weight changes of the mice in each group throughout the experiment. D-F) The appearance and morphology of the livers of mice in the sh-NC and sh-PTPRG-AS1 groups, the results of H&E staining and IHC staining of liver tissues, and the KITLG content in mouse serum, as determined by ELISA. G) Schematic diagram of the experimental protocol showing the effect of PTPRG-AS1 overexpression on GC liver metastasis. H) MRI monitoring of GC liver metastasis. I) Body weight changes of the mice in each group throughout the experiment. J–L) Appearance and morphology of the livers of mice in the vector and OE-PTPRG-AS1 groups, the results of H&E staining and IHC staining of liver tissues, and the KITLG content in mouse serum determined by ELISA. M-O) The relative RNA expression levels of PTPRG-AS1, hsa-miR-421, and KITLG were analyzed in GC liver metastatic nest tissues after knockdown or overexpression of PTPRG-AS1. Additionally, the relative expression levels of KITLG proteins and proteins related to the KITLG/KIT pathway were examined. Statistical analyses were performed using unpaired Student's *t*-tests for comparisons between two groups and one-way ANOVA with Tukey's HSD post hoc tests for multi-group comparisons. The data are presented as *mean* ± *SD*. Compared with the sh-NC group (or the vector group), *: $P < 0.05$, **: $P < 0.01$, $n = 6$.

ability, and treatment resistance [44–47]. Chemotherapy drugs can slow the growth of GC cells, but they may also push the cells into a dormant phase, increasing the risk of recurrence. Chemotherapy can also have negative effects on the patient health and quality of life [9,48–50]. Matrine, oxymatrine, sophoridine, and other compounds contained in CKI have been reported to have anti-GC cell survival and proliferation effects [51–53]. We obtained similar results in a study of GC cells treated with matrine [54]. According to the characteristics and safety of drugs, combinations of multiple compound drugs can often achieve better efficacy. CKI is a mixture containing a variety of compounds, and a compound formula based on the theory of traditional Chinese medicine. Aung et al. utilized the "subtractive fractionation approach" to analyze the chemical constituents of CKI and demonstrated that CKI contains a lower concentration of any single compound but still achieves the same level of effectiveness. It is important to note that this efficacy is a result of the combined action of multiple compounds in CKI, that act on various targets and utilize different mechanisms [55,56]. Similarly, we found that CKI has a comprehensive intervention effect on GC, which is reflected in changes in multiple GC phenotypes. CKI inhibits GC cell proliferation, DNA replication, colony formation, and cell cycle progression *in vitro*, while also reducing tumor volume and burden, decreasing GC cell survival and metastasis, and exhibiting immunomodulatory properties *in vivo*. Additionally, the IC_{50} values of CKI were lower in HGC-27 and MKN-45 GC cell lines than in other cell lines, indicating that these cells are more sensitive to CKI and could be useful for identifying the specific mechanisms of CKI intervention in GC.

The ceRNA network includes both mRNAs and ncRNAs, with only mRNAs being directly annotated and enriched. Therefore, it is inappropriate to investigate the mechanism by which CKI affects GC through only by mRNA or protein expression due to its multiple effects and mechanisms. Notably, an increasing number of ncRNAs, particularly lncRNAs, have been demonstrated to possess significant biological activity in GC and multiple tumors [57–60]. Therefore, we have incorporated ncRNAs into the analysis of the mechanism of CKI intervention in GC. The formation of a ceRNA mechanism between ncRNA and mRNA is considered one of the primary mechanisms through which ncRNA exerts its biological activity [58,61,62]. The ceRNA network, formed by the ceRNA axis, demonstrates the extensive range of regulation and strong regulatory abilities of ncRNAs [63,64]. At present, the annotation and enrichment analysis of the reported ceRNA network is limited to the mRNA components within the network [65–67]. This approach overlooks the potential impact of ncRNAs within the network. To address this limitation, we devised a simple method to annotate and enrich the entire ceRNA network, taking into account the role of ncRNA, to offer a more comprehensive understanding of its biological relevance. We designated this as the ceRNA network score (CNScore). In basic terms, the CNScore converts all nodes within the ceRNA network into scores for each GC patient. These scores are integrated with the gene expression profiles and clinical parameters of GC patients to obtain a comprehensive understanding of the biological and clinical significance of the ceRNA network. We focused on the proliferation and metastasis of GC using the CNScore method. Subsequently, we found that the PTPRG-AS1/miR-421/KITLG axis, as a key ceRNA axis, is a major contributor to the main biological functions mediated by the hub CKI-GC ceRNA network. Interestingly, the downstream KITLG/KIT pathway regulated by this axis can simultaneously regulate the proliferation and EMT of GC, and EMT is the key step in promoting GC metastasis. The RT-qPCR results showed that the expression of PTPRG-AS1, hsa--miR-421, and KITLG in HGC-27 and MKN-45 GC cells was more pronounced than that in other GC cells, suggesting a potential reason for their sensitivity to CKI intervention. The above results indicate that CKI inhibits the malignant progression of GC proliferation and metastasis by regulating the PTPRG-AS1/miR-421/KITLG axis to inhibit the KITLG/-KIT pathway. Conversely, this axis promotes the malignant progression of GC through the KITLG/KIT pathway.

The high malignancy of GC is evident in its rapid progression and metastasis, which is a significant contributing factor to the high mortality rate associated with this disease [6,7]. The rapid progression of GC can be attributed to the high level of proliferation of GC cells, as well as their possession of a complete set of metastatic programs (seeding and colonization), including the ability to easily migrate from the primary lesion, survive independently after detaching from the primary lesion, and invade and colonize other tissues [68]. EMT is correlated with detachment from the primary lesion. The proteins KIT, c-MYC, and β-catenin are associated with the capacity to survive independently. On the other hand, mesenchymal-epithelial transition (MET) is linked to the ability to colonize [69]. Coincidentally, the downstream targets of the KITLG/KIT pathway are implicated in the aforementioned processes. Tyrosine kinase receptor-specific ligand (KITLG), also referred to as stem cell factor (SCF), was initially discovered by Martin in 1990. KITLG has been shown the ability to augment the proliferation of myeloid and lymphoid hematopoietic progenitor cells in bone marrow culture [70]. There are two forms of KITLG: soluble and membrane-bound. Both forms have biological activity. Furthermore, KITLG is the exclusive ligand for the tyrosine kinase receptor c-KIT (CD117) and is also a pleiotropic factor. It produces various biological effects by binding to the receptor KIT, hence it is referred to as the KITLG/KIT signaling pathway [71]. It has been reported that this signaling pathway plays a significant role in multiple types of tumors. Chen et al. discovered a KIT^{+} subtype of colon cancer cells that activate the KITLG/KIT pathway, promoting tumor growth in mice [72]. Similarly, KITLG/KIT signaling is also found to be overactive in human meningiomas [73]. Brittni et al. found that high KITLG expression in adult stomachs on a human tissue microarray, particularly in men, is similar to the epidemiology of GC [71]. In addition, gastrointestinal stromal tumors usually have gain-of-function mutations in KIT and abnormal activation of the KITLG/KIT pathway [74],

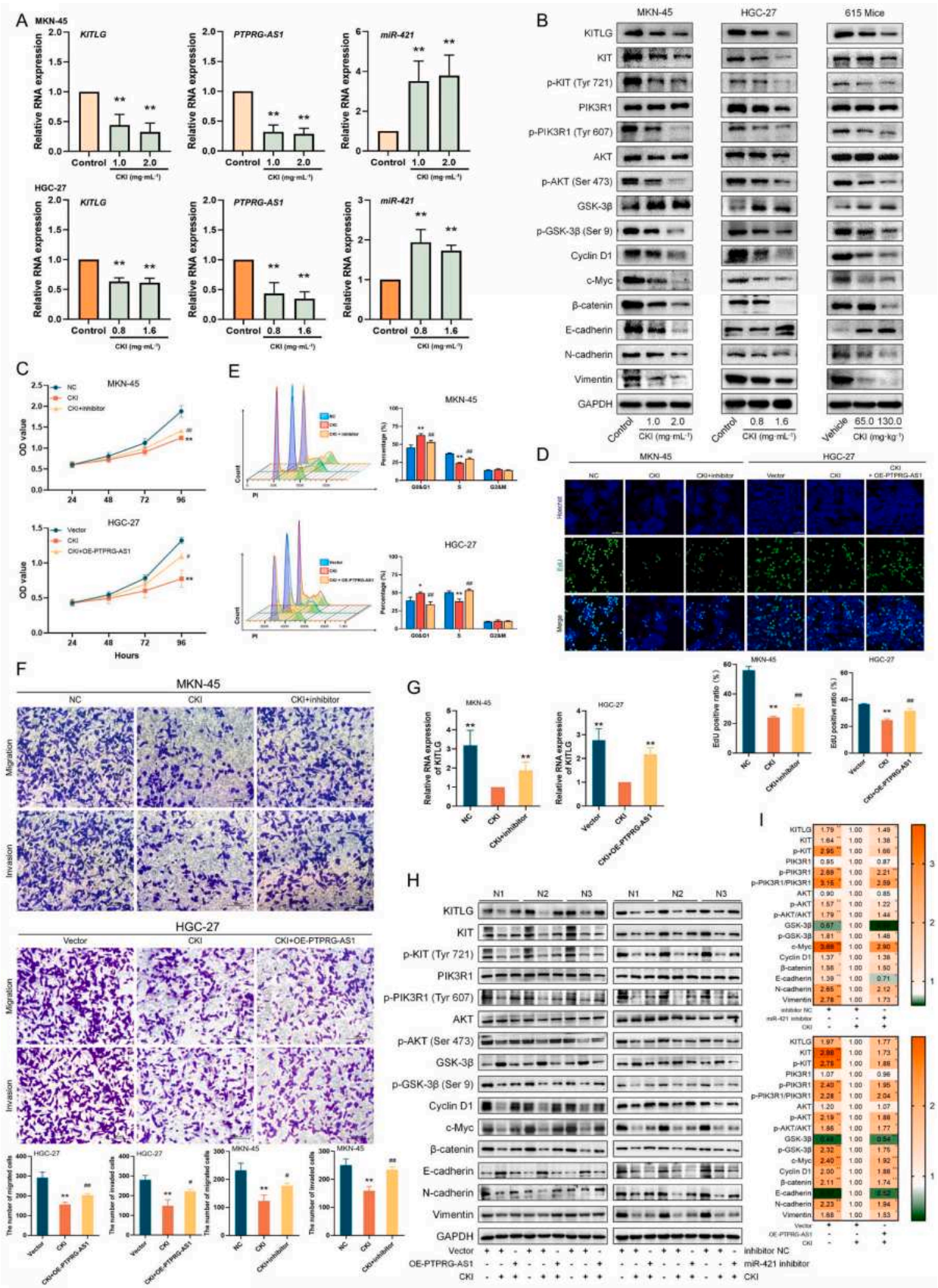

(caption on next page)

Fig. 9. CKI modulates PTPRG-AS1/hsa-miR-421/KITLG axis *in vitro*, downregulates KITLG/KIT pathway, inhibiting the malignant behavior of GC. A-B) Relative RNA expression of PTPRG-AS1, hsa-miR-421, and KITLG in MKN-45 and HGC-27 cells, as well as the relative expression of KITLG proteins and KITLG/KIT pathway-related proteins after CKI intervention. The relative expression of KITLG proteins and KITLG/KIT pathway-related proteins in subcutaneous tumor tissues after CKI intervention was measured. C–E) The CCK-8 assay, EdU incorporation assay, and ow cytometry were used to assess the effects of CKI on the proliferation of MKN-45 cells transiently transfected with hsa-miR-421 inhibitor or inhibitor NC or HGC-27 cells stably transfected with OE-PTPRG-AS1 or vector. Scale bar = 50 μm. F) The effect of CKI on cell migration and invasion ability was assessed in MKN-45 cells transiently transfected with the hsa-miR-421 inhibitor or the inhibitor NC or in HGC-27 cells stably transfected with OE-PTPRG-AS1 or vector using Transwell assays. Scale bar = 100 μm. G-I) RT-qPCR and Western blotting were used to detect the effect of CKI on the relative expression of KITLG in MKN-45 cells transiently transfected with hsa-miR-421 inhibitor or inhibitor NC or in HGC-27 cells stably transfected with OE-PTPRG-AS1 or vector and the relative expression of KITLG/KIT pathway-related proteins. Statistical analyses were performed using unpaired Student's *t*-tests for comparisons between two groups and one-way ANOVA with Tukey's HSD post hoc tests for multi-group comparisons. The data are presented as *mean* ± *SD*. Compared with the NC group (or the vector group), *: $P < 0.05$, **: $P < 0.01$, ***: $P < 0.001$. Compared with the CKI group, #: $P < 0.05$, ##: $P < 0.01$, $n = 3$.

suggesting that the KITLG/KIT pathway may play an important role in the occurrence and development of GC. However, no reports have con rmed this connection. In our study, upregulating the KITLG/KIT pathway enhanced GC proliferation and metastasis, while downregulating this pathway inhibited these processes. CKI inhibits GC proliferation and metastasis by targeting the KITLG/KIT pathway. Therefore, we believe that the abnormal activation of the KITLG/KIT pathway is one of the important reasons for the malignant proliferation and metastasis of GC, and it is also one of the important pathways targeted by CKI to inhibit the malignant progression of GC.

Protein tyrosine phosphatase, receptor type G, antisense (PTPRG-AS1) refers to the complementary strand of the PTPRG gene. Initial ndings indicate that the expression of PTPRG-AS1 is associated with ER^+ and ER^- subtypes, tumor histology grade, and clinical outcomes in patients with breast cancer. Consequently, it holds promise as a potential biomarker for breast cancer diagnosis [75]. Li et al. reported that the oncogene POU2F2 can transcriptionally enhance the expression of PTPRG-AS1, which targets the miR-376c-3p/SLC7A11 axis to inhibit ferroptosis in triple negative breast cancer cells thereby promoting cancer progression [76]. Subsequently, PTPRG-AS1 was found to play an important role in a variety of tumors through a ceRNA mechanism. PTPRG-AS1 is upregulated in non-small cell lung cancer tissues, competing with TCF4 for miR-200c-3p to upregulate TCF4 expression and promote the survival and radioresistance of cancer cells [77]. Similarly, the two ceRNA axes PTPRG-AS1/miR-124–3p/LHX2 and PTPRG-AS1/miR-194–3p/PRC1 showed resistance to radiotherapy in nasopharyngeal carcinoma cells [78,79]. In osteosarcoma, PTPRG-AS1 promotes cancer cell metastasis and predicts a poor outcome [80]. Currently, only one article has shown that PTPRG-AS1 is upregulated in GC tissue samples and indicates a poor prognosis [81]. Furthermore, there have been no reports linking PTPRG-AS1 to GC, thus the signi - cance of PTPRG-AS1 in relation to GC remains unclear.

To the best of our knowledge, this study represents the initial discovery and demonstration of PTPRG-AS1 as a functional lncRNA in GC. Overall, we suggest that PTPRG-AS1 is a GC risk gene. The OS, DSS, and PFI curves for PTPRG-AS1 indicate that higher PTPRG-AS1 expression is associated with a poorer prognosis. We knocked down PTPRG-AS1 in GC cells, which decreased their viability, DNA replication ability, S-phase cell ratio, migration, and invasion. This also reduced the volume of GC metastases in the livers of mice and the number of metastatic cancer nests. The KITLG/KIT pathway was suppressed. Conversely, overexpressing PTPRG-AS1 in GC cells had the opposite effects. These nd-ings strongly suggest that PTPRG-AS1, a GC risk gene, promotes the malignant progression of GC proliferation and metastasis through the KITLG/KIT pathway. Our study revealed that PTPRG-AS1 targets the hsa-miR-421/KITLG axis in GC, leading to similar effects on cell cycle arrest and malignant proliferation. Additionally, Cyclin D1, encoded by the CCND1 gene, is a downstream target of the KITLG/KIT pathway. This suggests that PTPRG-AS1 is involved in multiple pathways and targets. Consequently, our study provides evidence for the wide-ranging and signi cant impact of the ceRNA network. Some scholars believe that hsa-miR-421 is a GC risk gene [82,83]. This nding contradicts the results of our research. Nevertheless, it is important to note that controversial ndings are frequently encountered, particularly in reports related to molecular oncology. We hypothesize that the main contributing factor could be the heterogeneity of GC. It is plausible that the various states and ecotypes of GC cells may result in hsa-miR-421 displaying both pro-cancer and anti-cancer effects [84]. The secondary reason could be attributed to the limitations of a single molecule. Liu et al. discovered that hsa-miR-421 exhibits high sensitivity in diagnosing GC, however, its speci city is considerably low [85]. Manoel-Caetano et al. reported that the comprehensive effect of the mRNA-miRNA network should be considered, as hsa-miR-421 is both positively correlated with base excision repair and negatively correlated with DNA damage response [86]. Therefore, we speculate that it may be more convincing to combine all nodes in the hub CKI-GC ceRNA network for the diagnosis of GC. We used hsa-miR-421 mimics to replicate the phenotype and KITLG/KIT pathway downregulation produced by PTPRG-AS1 knockdown. However, hsa-miR-421 inhibition had the opposite effects. Subsequently, we used a dual-luciferase reporter gene assay to con rm that there was MRE binding between PTPRG-AS1 and hsa-miR-421, and between hsa-miR-421 and KITLG. Furthermore, in the rescue experiment, hsa-miR-421 mimics signi cantly attenuated the malignant proliferation and metastasis of GC caused by PTPRG-AS1 overexpression, accompanied by a decrease in the activity of the KITLG/KIT pathway. Conversely, hsa-miR-421 inhibition signi cantly attenuated PTPRG-AS1 knockdown-induced inhibition of GC malignancy, accompanied by the recovery of KITLG/KIT pathway activity. Similarly, overexpression of PTPRG-AS1 or hsa-miR-421 inhibition signi cantly reduced the inhibitory effect of CKI on the malignant progression of GC, accompanied by the recovery of KITLG/KIT pathway activity. In terms of the current reports, we are the rst to comprehensively report on the role and mechanism of CKI intervention in GC. Additionally, we are the rst to comprehensively study the expression, function, regulatory mechanism, and clinical signi cance of the lncRNA PTPRG-AS1 in GC. However, due to the limitations of this study, we were unable to utilize all the nodes in the hub CKI-GC ceRNA network to monitor the malignant progression of GC. This is a research direction that we will explore in the future.

5. Conclusions

We discovered and provided evidence that the lncRNA PTPRG-AS1 plays a role in promoting the malignant progression of GC by targeting the hsa-miR-421/KITLG axis and increasing the expression of the KITLG/KIT pathway. Additionally, CKI has the ability to regulate the PTPRG-AS1/hsa-miR-421/KITLG axis and decrease the expression of the KITLG/KIT pathway, thereby inhibiting the malignant proliferation and

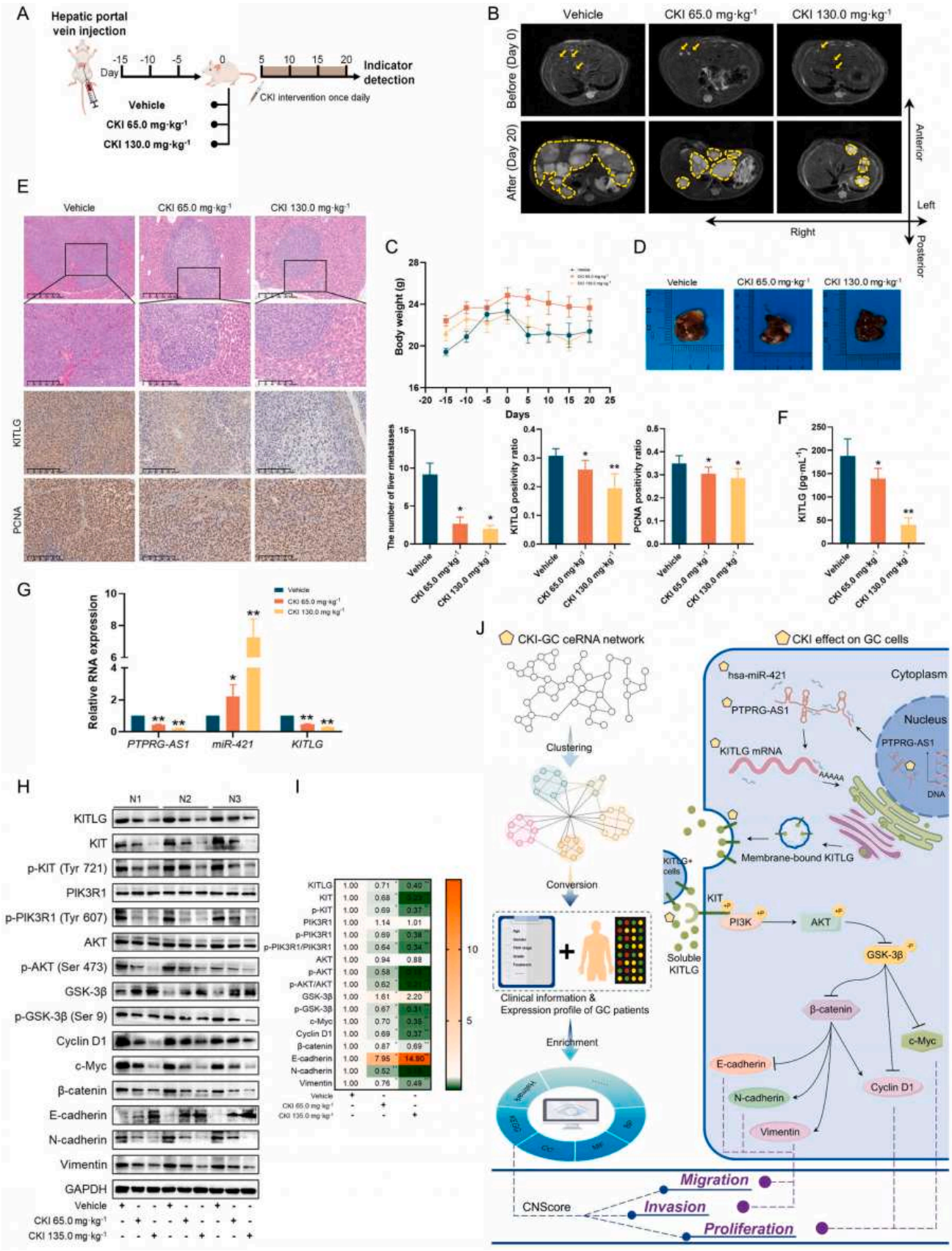

(caption on next page)

Fig. 10. CKI regulates PTPRG-AS1/hsa-miR-421/KITLG axis, downregulates KITLG/KIT pathway *in vivo*, inhibits GC growth, proliferation and metastasis. A) Schematic diagram of the experimental protocol showing the effect of CKI on GC liver metastasis. B) MRI monitoring of GC liver metastasis. C) Body weight changes of the mice in each group throughout the experiment. D-F) The liver appearance and morphology of the vehicle group, CKI 65.0 mg kg^{-1} group and CKI 130.0 mg kg^{-1} group were assessed through H&E staining and IHC staining of liver tissues, as well as by determining the KITLG content in mouse serum using ELISA. G-I) Relative RNA expression of PTPRG-AS1, hsa-miR-421, and KITLG, as well as the relative expression of KITLG protein and KITLG/KIT pathway-related proteins in GC liver metastasis nest tissues after CKI intervention. Statistical analyses were performed using unpaired Student's *t*-tests for comparisons between two groups and one-way ANOVA with Tukey's HSD post hoc tests for multi-group comparisons. The data are presented as *mean* ± *SD*. Compared with the vehicle group, *: $P < 0.05$, **: $P < 0.01$, $n = 6$. J) A summary schema of the mechanism of this study: the PTPRG-AS1 sponge adsorbs hsa-miR-421 and thus releases KITLG, which in turn upregulates the KITLG/KIT pathway to promote malignant growth, proliferation, and metastasis of GC. CKI inhibits the malignant progression of GC by regulating the PTPRG-AS1/hsa-miR-421/KITLG axis.

metastasis of GC. Our work revealed that CKI has clinical signi cance in the prevention and treatment of GC metastasis. Moreover, it offers valuable insights into the underlying mechanisms of malignant progression of GC and aids in the development of improved treatment strategies for this disease.

CRediT authorship contribution statement

Jiarui Wu: Writing – review & editing, Project administration, Funding acquisition. **Jingyuan Zhang:** Visualization. **Fanqin Zhang:** Validation, Formal analysis. **Siyu Guo:** Visualization. **Shan Lu:** Validation, Formal analysis. **Xiaomeng Zhang:** Writing – review & editing. **Yifei Gao:** Writing – original draft, Validation, Methodology, Formal analysis. **Xinkui Liu:** Writing – review & editing. **Chao Wu:** Writing – original draft, Validation, Methodology, Formal analysis, Conceptualization. **Xiaoyu Tao:** Visualization. **Jiaqi Huang:** Validation, Formal analysis. **Haojia Wang:** Visualization. **Qinglin Li:** Writing – review & editing. **Zhihong Huang:** Validation, Formal analysis, Conceptualization. **Leiming You:** Writing – review & editing. **Zhengsen Jin:** Writing – original draft, Validation, Methodology, Formal analysis.

Ethics approval and consent to participate

All animal experiments were approved by the Animal Ethics Committee of Beijing University of Chinese Medicine (Ethics number: BUCM-2022010502-1130, BUCM-2023020302-1127), and conducted in accordance with the WMA Statement on animal use in biomedical research and the EU recommendations (Directive 2010/63/EU) for experimental design and analysis in pharmacology care.

Funding

The design of the study and the collection, analysis, and interpretation of data were supported by the National Natural Science Foundation of China (No. 82074284, China), the State Administration of Traditional Chinese Medicine High-level Key Discipline Construction Project - Clinical Chinese Pharmacy (No. zyyzdxk-2023257, China), and the Innovation Team and Talents Cultivation Program of National Administration of Traditional Chinese Medicine (No. ZYYCXTD-C-202005, China).

Declaration of Competing Interest

The authors declare that they have no competing interests.

Appendix A. Supporting information

Supplementary data associated with this article can be found in the online version at doi:10.1016/j.phrs.2025.107743.

Data availability

Data will be made available on request.

References

[1] S.S. Joshi, B.D. Badgwell, Current treatment and recent progress in gastric cancer, CA: A Cancer J. Clin. 71 (2021) 264–279.
[2] E.C. Smyth, M. Nilsson, H.I. Grabsch, N.C. van Grieken, F. Lordick, Gastric cancer, Lancet 396 (2020) 635–648.
[3] Z. Wang, W. Han, F. Xue, Y. Zhao, P. Wu, Y. Chen, C. Yang, W. Gu, J. Jiang, Nationwide gastric cancer prevention in china, 2021-2035: a decision analysis on effect, affordability and cost-effectiveness optimisation, Gut 71 (2022) 2391–2400.
[4] H. Zeng, X. Ran, L. An, R. Zheng, S. Zhang, J.S. Ji, Y. Zhang, W. Chen, W. Wei, J. He, HBCR Working Group, Disparities in stage at diagnosis for ve common cancers in china: a multicentre, hospital-based, observational study, Lancet Public Health 6 (2021) e877–e887.
[5] T. Ugai, N. Sasamoto, H. Lee, M. Ando, M. Song, R.M. Tamimi, I. Kawachi, P. T. Campbell, E.L. Giovannucci, E. Weiderpass, T.R. Rebbeck, S. Ogino, Is early-onset cancer an emerging global epidemic? Current evidence and future implications, Nat. Rev. Clin. Oncol. 19 (2022) 656–673.
[6] Y. Gao, H. Xi, L. Shang, Z. Tang, B. Wei, Z. Qiao, Y. Tang, X. Wang, J. Zhou, X. Wang, C. Huang, J. Lu, G. Li, J. Yu, Y. Liang, J. Ji, Z. Li, K. Xue, H. Liang, B. Ke, L. Zang, Z. He, S. Xie, H. Huang, Z. Xu, Y. Tian, J. Xiong, J. Li, Q. Cui, L. Li, T. Lu, Q. Song, S. Liu, Y. Sun, L. Li, L. Chen, RECORD study group, Clinical landscape and prognosis of patients with gastric cancer liver metastases: a nation-wide multicenter cohort study in china (record study), Sci. Bull. 69 (2023) 303–307.
[7] C.L. Chaffer, R.A. Weinberg, A perspective on cancer cell metastasis, Science 331 (2011) 1559–1564.
[8] S. Li, W. Yu, F. Xie, H. Luo, Z. Liu, W. Lv, D. Shi, D. Yu, P. Gao, C. Chen, M. Wei, W. Zhou, J. Wang, Z. Zhao, X. Dai, Q. Xu, X. Zhang, M. Huang, K. Huang, J. Wang, J. Li, L. Sheng, L. Liu, Neoadjuvant therapy with immune checkpoint blockade, antiangiogenesis, and chemotherapy for locally advanced gastric cancer, Nat. Commun. 14 (2023) 8–16.
[9] W. Guan, Y. He, R. Xu, Gastric cancer treatment: recent progress and future perspectives, J. Hematol. Oncol. 16 (2023) 57.
[10] Y.Y. Janjigian, K. Shitara, M. Moehler, M. Garrido, P. Salman, L. Shen, L. Wyrwicz, K. Yamaguchi, T. Skoczylas, A. Campos Bragagnoli, T. Liu, M. Schenker, P. Yanez, M. Tehfe, R. Kowalyszyn, M.V. Karamouzis, R. Bruges, T. Zander, R. Pazo-Cid, E. Hitre, K. Feeney, J.M. Cleary, V. Poulart, D. Cullen, M. Lei, H. Xiao, K. Kondo, M. Li, J.A. Ajani, First-line nivolumab plus chemotherapy versus chemotherapy alone for advanced gastric, gastro-oesophageal junction, and oesophageal adenocarcinoma (checkmate 649): a randomised, open-label, phase 3 trial, Lancet 398 (2021) 27–40.
[11] S. Al-Batran, T.O. Goetze, D.W. Mueller, A. Vogel, M. Winkler, S. Lorenzen, A. Novotny, C. Pauligk, N. Homann, T. Jungbluth, C. Reissfelder, K. Caca, S. Retter, E. Horndasch, J. Gumpp, C. Bolling, K.H. Fuchs, W. Blau, W. Padberg, M. Pohl, A. Wunsch, P. Michl, F. Mannes, M. Schwarzbach, H. Schmalenberg, M. Hohaus, C. Scholz, C. Benckert, J.R. Knorrenschild, V. Kanngießer, T. Zander, H. Alakus, R. D. Hofheinz, C. Roedel, M.A. Shah, M. Sasako, D. Lorenz, J. Izbicki, W. O. Bechstein, H. Lang, S.P. Moenig, The renaissance (aio- ot5) trial: effect of chemotherapy alone vs. Chemotherapy followed by surgical resection on survival and quality of life in patients with limited-metastatic adenocarcinoma of the stomach or esophagogastric junction - a phase III trial of the german aio/cao-v/caogi, BMC Cancer 17 (2017) 893.
[12] Y. Zeng, R.U. Jin, Molecular pathogenesis, targeted therapies, and future perspectives for gastric cancer, Semin. Cancer Biol. 86 (2017) 566–582.
[13] F. Lordick, F. Carneiro, S. Cascinu, T. Fleitas, K. Haustermans, G. Piessen, A. Vogel, E.C. Smyth, ESMO Guidelines Committee, Electronic address: clinicalguidelines@esmo.org, Gastric cancer: esmo clinical practice guideline for diagnosis, treatment and follow-up, Ann. Oncol. 33 (2022) 1005–1020.
[14] F.H. Wang, X.T. Zhang, Y.F. Li, L. Tang, X.J. Qu, J.E. Ying, J. Zhang, L.Y. Sun, R. B. Lin, H. Qiu, C. Wang, M.Z. Qiu, M.Y. Cai, Q. Wu, H. Liu, W.L. Guan, A.P. Zhou, Y.J. Zhang, T.S. Liu, F. Bi, X.L. Yuan, S.X. Rao, Y. Xin, W.Q. Sheng, H.M. Xu, G. X. Li, J.F. Ji, Z.W. Zhou, H. Liang, Y.Q. Zhang, J. Jin, L. Shen, J. Li, R.H. Xu, The chinese society of clinical oncology (csco): clinical guidelines for the diagnosis and treatment of gastric cancer, 2021, Cancer Commun. 41 (2021) 747–795.
[15] H. Gou, H. Su, D. Liu, C.C. Wong, H. Shang, Y. Fang, X. Zeng, H. Chen, Y. Li, Z. Huang, M. Fan, C. Wei, X. Wang, X. Zhang, X. Li, J. Yu, Traditional medicine pien tze huang suppresses colorectal tumorigenesis through restoring gut microbiota and metabolites, Gastroenterology 165 (2023) 1404–1419.
[16] L. Wang, G. Zhou, P. Liu, J. Song, Y. Liang, J.X. Yan, F. Xu, B.S. Wang, J.H. Mao, Z. X. Shen, S.J. Chen, Z. Chen, Dissection of mechanisms of chinese medicinal formula realgar-indigo naturalis as an effective treatment for promyelocytic leukemia, Proc. Natl. Acad. Sci. USA 105 (2008) 4826–4831.

[17] Y. Yang, K. Feng, L. Yuan, Y. Liu, M. Zhang, K. Guo, Z. Yin, W. Wang, S. Zhou, H. Sun, K. Yan, X. Yan, X. Wang, Y. Duan, Y. Hu, J. Han, Compound danshen dripping pill inhibits hypercholesterolemia/atherosclerosis-induced heart failure in apoe and ldlr dual de cient mice via multiple mechanisms, Acta Pharm. Sin. B 13 (2023) 1036–1052.
[18] Z. Zhao, H. Fan, T. Higgins, J. Qi, D. Haines, A. Trivett, J.J. Oppenheim, H. Wei, J. Li, H. Lin, O.M. Howard, Fufang kushen injection inhibits sarcoma growth and tumor-induced hyperalgesia via trpv1 signaling pathways, Cancer Lett. 355 (2014) 232–241.
[19] W. Wang, R.L. You, W.J. Qin, L.N. Hai, M.J. Fang, G.H. Huang, R.X. Kang, M.H. Li, Y.F. Qiao, J.W. Li, A.P. Li, Anti-tumor activities of active ingredients in compound kushen injection, Acta Pharmacol. Sin. 36 (2015) 676–679.
[20] W. Xu, H. Lin, Y. Zhang, X. Chen, B. Hua, W. Hou, X. Qi, Y. Pei, X. Zhu, Z. Zhao, L. Yang, Compound kushen injection suppresses human breast cancer stem-like cells by down-regulating the canonical wnt/β-catenin pathway, J. Exp. Clin. Cancer Res. 30 (2011) 103.
[21] M. Ao, X. Xiao, Q. Li, Ef cacy and safety of compound kushen injection combined with chemotherapy on postoperative patients with breast cancer, Medicine 98 (2019) e14024.
[22] X. Wang, J. Liu, H. Lin, W. Hou, A multicenter randomized controlled open-label trial to assess the ef cacy of compound kushen injection in combination with single-agent chemotherapy in treatment of elderly patients with advanced non-small cell lung cancer: study protocol for a randomized controlled trial, Trials 17 (2016) 124.
[23] H. Tu, B. Lei, S. Meng, H. Liu, Y. Wei, A. He, W. Zhang, F. Zhou, Ef cacy of compound kushen injection in combination with induction chemotherapy for treating adult patients newly diagnosed with acute leukemia, Evid. Based Complement. Altern. Med. 2016 (2016) 1–7.
[24] L. Yu, Y. Zhou, Y. Yang, F. Lu, Y. Fan, Ef cacy and safety of compound kushen injection on patients with advanced colon cancer: a meta-analysis of randomized controlled trials, Evid. Based Complement. Altern. Med. 2017 (2017) 1–9.
[25] C. Li, D. Niu, R. Zhu, X. Yan, H. Qu, Y. Zhang, Y. Zheng, Adjunctive effect of compound kushen injection for cancer: an overview of systematic reviews, J. Ethnopharmacol. 317 (2023) 116778.
[26] Z. Huang, P. Wei, Compound kushen injection for gastric cancer, Medicine 98 (2019) e17927.
[27] J. Zhang, Z. Qu, H. Yao, L. Sun, Y. Harata-Lee, J. Cui, T.N. Aung, X. Liu, R. You, W. Wang, L. Hai, D.L. Adelson, L. Lin, An effective drug sensitizing agent increases ge tinib treatment by down regulating pi3k/akt/mtor pathway and up regulating autophagy in non-small cell lung cancer, Biomed. Pharmacother. 118 (2019) 109169.
[28] Y. Yang, M. Sun, W. Yao, F. Wang, X. Li, W. Wang, J. Li, Z. Gao, L. Qiu, R. You, C. Yang, Q. Ba, H. Wang, Compound kushen injection relieves tumor-associated macrophage-mediated immunosuppression through tnfr1 and sensitizes hepatocellular carcinoma to sorafenib, J. Immunother. Cancer 8 (2019) e317.
[29] Y. Yang, M. Sun, W. Li, C. Liu, Z. Jiang, P. Gu, J. Li, W. Wang, R. You, Q. Ba, X. Li, H. Wang, Rebalancing tgf - β/smad7 signaling via compound kushen injection in hepatic stellate cells protects against liver brosis and hepatocarcinogenesis, Clin. Transl. Med. 11 (2021) e410.
[30] J.T. Lee, Epigenetic regulation by long noncoding rnas, Science 338 (2012) 1435–1439.
[31] T. Nojima, N.J. Proudfoot, Mechanisms of lncrna biogenesis as revealed by nascent transcriptomics, Nat. Rev. Mol. Cell Biol. 23 (2022) 389–406.
[32] S. Ma, M. Zhou, Y. Xu, X. Gu, M. Zou, G. Abudushalamu, Y. Yao, X. Fan, G. Wu, Clinical application and detection techniques of liquid biopsy in gastric cancer, Mol. Cancer 22 (2023) 7.
[33] S. Adnane, A. Marino, E. Leucci, Lncrnas in human cancers: signal from noise, Trends Cell Biol. 32 (2023) 565–573.
[34] T.R. Cech, J.A. Steitz, The noncoding rna revolution—trashing old rules to forge new ones, Cell 157 (2014) 77–94.
[35] L. Salmena, L. Poliseno, Y. Tay, L. Kats, P.P. Pandol , A cerna hypothesis: the rosetta stone of a hidden rna language? Cell 146 (2011) 353–358.
[36] Y. Tay, J. Rinn, P.P. Pandol , The multilayered complexity of cerna crosstalk and competition, Nature 505 (2014) 344–352.
[37] J. Wan, Z. Zhang, C. Wu, S. Tian, Y. Zang, G. Jin, Q. Sun, P. Wang, X. Luan, Y. Yang, X. Zhan, L.L. Ye, D.D. Duan, X. Liu, W. Zhang, Astragaloside iv derivative hhq16 ameliorates infarction-induced hypertrophy and heart failure through degradation of lncrna4012/9456, Signal Transduct. Target Ther. 8 (2023) 414.
[38] C. Wang, Y. Chen, Y. Wang, X. Liu, Y. Liu, Y. Li, H. Chen, C. Fan, D. Wu, J. Yang, Inhibition of cox-2, mpges-1 and cyp4a by isoliquiritigenin blocks the angiogenic akt signaling in glioma through cerna effect of mir-194-5p and lncrna neat1, J. Exp. Clin. Cancer Res. 38 (2019) 371.
[39] F. Wang, C. Yuan, B. Liu, Y. Yang, H. Wu, Syringin exerts anti-breast cancer effects through pi3k-akt and egfr-ras-raf pathways, J. Transl. Med. 20 (2022) 310.
[40] W. Zhou, C. Wu, C. Zhao, Z. Huang, S. Lu, X. Fan, Y. Tan, A. Stalin, R. You, X. Liu, J. Zhang, Z. Wu, J. Wu, An advanced systems pharmacology strategy reveals akr1b1, mmp2, ptger3 as key genes in the competing endogenous rna network of compound kushen injection treating gastric carcinoma by integrated bioinformatics and experimental veri cation, Front. Cell. Dev. Biol. 9 (2021) 742421.
[41] Z. Huang, C. Wu, W. Zhou, S. Lu, Y. Tan, Z. Wu, R. You, A. Stalin, F. Guo, J. Zhang, P. Liu, W. Wang, X. Duan, L. You, J. Wu, Compound kushen injection inhibits epithelial-mesenchymal transition of gastric carcinoma by regulating vcam1 induced by the tnf signaling pathway, Phytomedicine 118 (2023) 154984.
[42] Z. Luo, Z. Rong, J. Zhang, Z. Zhu, Z. Yu, T. Li, Z. Fu, Z. Qiu, C. Huang, Circular rna circccdc9 acts as a mir-6792-3p sponge to suppress the progression of gastric cancer through regulating cav1 expression, Mol. Cancer 19 (2020) 86.
[43] K. Wang, X. Zhao, J. Liu, R. Zhang, J. Li, Nervous system and gastric cancer, Biochim. Et. Biophys. Acta (BBA) - Rev. Cancer 1873 (2020) 188313.
[44] B. Chen, W.N. Chan, C.W. Mui, X. Liu, J. Zhang, Y. Wang, A.H.K. Cheung, A.K. Y. Chan, R.C.K. Chan, K.T. Leung, Y. Dong, Y. Pan, H. Ke, L. Liang, Z. Zhou, C. C. Wong, W.K.K. Wu, A.S.L. Cheng, J. Yu, K.W. Lo, K.F. To, W. Kang, Stk3 promotes gastric carcinogenesis by activating ras-mapk mediated cell cycle progression and serves as an independent prognostic biomarker, Mol. Cancer 20 (2021) 147.
[45] K. Kim, H. Huang, P.K. Parida, L. He, M. Marquez-Palencia, T.C. Reese, P. Kapur, J. Brugarolas, R.A. Brekken, S. Malladi, Cell competition shapes metastatic latency and relapse, Cancer Discov. 13 (2021) 85–97.
[46] H.H.N. Yan, H.C. Siu, S. Law, S.L. Ho, S.S.K. Yue, W.Y. Tsui, D. Chan, A.S. Chan, S. Ma, K.O. Lam, S. Bartfeld, A.H.Y. Man, B.C.H. Lee, A.S.Y. Chan, J.W.H. Wong, P. S.W. Cheng, A.K.W. Chan, J. Zhang, J. Shi, X. Fan, D.L.W. Kwong, T.W. Mak, S. T. Yuen, H. Clevers, S.Y. Leung, A comprehensive human gastric cancer organoid biobank captures tumor subtype heterogeneity and enables therapeutic screening, Cell Stem Cell 23 (2018) 882–897.
[47] L. Wei, J. Sun, N. Zhang, Y. Zheng, X. Wang, L. Lv, J. Liu, Y. Xu, Y. Shen, M. Yang, Noncoding rnas in gastric cancer: implications for drug resistance, Mol. Cancer 19 (2018) 62.
[48] H. Jiang, D. Yu, P. Yang, R. Guo, M. Kong, Y. Gao, X. Yu, X. Lu, X. Fan, Revealing the transcriptional heterogeneity of organ-speci c metastasis in human gastric cancer using single-cell rna sequencing, Clin. Transl. Med. 12 (2022) e730.
[49] L. Seeneevassen, E. Bessède, F. Mégraud, P. Lehours, P. Dubus, C. Varon, Gastric cancer: advances in carcinogenesis research and new therapeutic strategies, Int. J. Mol. Sci. 22 (2021) 3418.
[50] M. Katoh, M. Katoh, Wnt signaling and cancer stemness, Essays Biochem. 66 (2022) 319–331.
[51] H.F. Hu, Z. Wang, W.L. Tang, X.M. Fu, X.J. Kong, Y.K. Qiu, S.Y. Xi, Effects of Sophora avescens aiton and the absorbed bioactive metabolite matrine individually and in combination with 5- uorouracil on proliferation and apoptosis of gastric cancer cells in nude mice, Front. Pharmacol. 13 (2022) 1047507.
[52] Y. Huang, J. Zhang, G. Wang, X. Chen, R. Zhang, H. Liu, J. Zhu, Oxymatrine exhibits anti-tumor activity in gastric cancer through inhibition of il-21r-mediated jak2/stat3 pathway, Int. J. Immunopathol. Pharmacol. 32 (2018) 1120488301.
[53] Z. Peng, Q. Guan, J. Luo, W. Deng, J. Liu, R. Yan, W. Wang, Sophoridine exerts tumor-suppressive activities via promoting esrrg-mediated β-catenin degradation in gastric cancer, BMC Cancer 20 (2018) 582.
[54] Y. Gao, C. Wu, J. Huang, Z. Huang, Z. Jin, S. Guo, X. Tao, S. Lu, J. Zhang, F. Zhang, Y. Zhai, R. Shi, P. Ye, J. Wu, A new strategy to identify adam12 and pdgfrb as a novel prognostic biomarker for matrine regulates gastric cancer via high throughput chip mining and computational veri cation, Comput. Biol. Med. 166 (2018) 107562.
[55] T.N. Aung, S. Nourmohammadi, Z. Qu, Y. Harata-Lee, J. Cui, H.Y. Shen, A.J. Yool, T. Pukala, H. Du, R.D. Kortschak, W. Wei, D.L. Adelson, Fractional deletion of compound kushen injection indicates cytokine signaling pathways are critical for its perturbation of the cell cycle, Sci. Rep. 9 (2019) 14200.
[56] S. Nourmohammadi, T.N. Aung, J. Cui, J.V. Pei, M.L. De Ieso, Y. Harata-Lee, Z. Qu, D.L. Adelson, A.J. Yool, Effect of compound kushen injection, a natural compound mixture, and its identi ed chemical components on migration and invasion of colon, brain, and breast cancer cell lines, Front. Oncol. 9 (2019) 314.
[57] D. Singh, Y.G. Assaraf, R.N. Gacche, Long non-coding rna mediated drug resistance in breast cancer, Drug Resist. Updat 63 (2022) 100851.
[58] S.A. Ali, M.J. Peffers, M.J. Ormseth, I. Jurisica, M. Kapoor, The non-coding rna interactome in joint health and disease, Nat. Rev. Rheumatol. 17 (2021) 692–705.
[59] F.J. Slack, A.M. Chinnaiyan, The role of non-coding rnas in oncology, Cell 179 (2021) 1033–1055.
[60] F. Kopp, J.T. Mendell, Functional classi cation and experimental dissection of long noncoding rnas, Cell 172 (2018) 393–407.
[61] Y. Zhang, X. Dong, X. Guo, C. Li, Y. Fan, P. Liu, D. Yuan, X. Ma, J. Wang, J. Zheng, H. Li, P. Gao, Lncrna-bc069792 suppresses tumor progression by targeting kcnq4 in breast cancer, Mol. Cancer 22 (2018) 41.
[62] Y. Wei, X. Tang, Y. Ren, Y. Yang, F. Song, J. Fu, S. Liu, M. Yu, J. Chen, S. Wang, K. Zhang, Y. Tan, Z. Han, L. Wei, B. Zhang, Z. Cheng, L. Li, H. Wang, An rna–rna crosstalk network involving hmgb1 and rictor facilitates hepatocellular carcinoma tumorigenesis by promoting glutamine metabolism and impedes immunotherapy by pd-l1+ exosomes activity, Signal Transduct. Target Ther. 6 (2021) 421.
[63] X. Xu, K. Wang, O. Vera, A. Verma, N. Jasani, I. Bok, O. Elemento, D. Du, X. Yu, F. A. Karreth, Gain of chromosome 1q perturbs a competitive endogenous rna network to promote melanoma metastasis, Cancer Res. 82 (2022) 3016–3131.
[64] S. Yang, X. Wang, X. Zhou, L. Hou, J. Wu, W. Zhang, H. Li, C. Gao, C. Sun, Ncrna-mediated cerna regulatory network: transcriptomic insights into breast cancer progression and treatment strategies, Biomed. Pharmacother. 162 (2023) 114698.
[65] S. Xue, B. Zheng, S. Cao, J. Ding, G. Hu, W. Liu, C. Chen, Long non-coding rna linc00680 functions as a cerna to promote esophageal squamous cell carcinoma progression through the mir-423-5p/pak6 axis, Mol. Cancer 21 (2022) 69.
[66] Z. Zhang, X. Huang, J. Yang, S. Gu, Y. Zhao, Y. Liu, Y. Khoong, S. Wang, S. Luo, T. Zan, G. Li, Identi cation and functional analysis of a three-mirna cerna network in hypertrophic scars, J. Transl. Med. 19 (2022) 451.
[67] L. Zheng, C. Xiang, X. Li, Q. Guo, L. Gao, H. Ni, Y. Xia, T. Xi, Stard13-correlated cerna network-directed inhibition on yap/taz activity suppresses stemness of breast cancer via co-regulating hippo and rho-gtpase/f-actin signaling, J. Hematol. Oncol. 11 (2018) 72.

[68] G. Bergers, S. Fendt, The metabolism of cancer cells during metastasis, Nat. Rev. Cancer 21 (2021) 162–180.
[69] A.W. Lambert, R.A. Weinberg, Linking emt programmes to normal and neoplastic epithelial stem cells, Nat. Rev. Cancer 21 (2021) 325–338.
[70] F.H. Martin, S.V. Suggs, K.E. Langley, H.S. Lu, J. Ting, K.H. Okino, C.F. Morris, I. K. McNiece, F.W. Jacobsen, E.A. Mendiaz, Primary structure and functional expression of rat and human stem cell factor dnas, Cell 63 (1990) 203–211.
[71] B.M. Foster, K.L. Langsten, A. Mansour, L. Shi, B.A. Kerr, Tissue distribution of stem cell factor in adults, Exp. Mol. Pathol. 122 (1990) 104678.
[72] E.C. Chen, T.A. Karl, T. Kalisky, S.K. Gupta, C.A. O Brien, T.A. Longacre, M. van de Rijn, S.R. Quake, M.F. Clarke, M.E. Rothenberg, Kit signaling promotes growth of colon xenograft tumors in mice and is up-regulated in a subset of human colon cancers, Gastroenterology 149 (2015) 705–717.
[73] M. Saini, A.N. Jha, A. Abrari, S. Ali, Expression of proto-oncogene kit is up-regulated in subset of human meningiomas, BMC Cancer 12 (2012) 212.
[74] Y. Hayashi, D.T. Asuzu, S.J. Gibbons, K.H. Aarsvold, M.R. Bardsley, G.A. Lomberk, A.J. Mathison, M.L. Kendrick, K.R. Shen, T. Taguchi, A. Gupta, B.P. Rubin, J. A. Fletcher, G. Farrugia, R.A. Urrutia, T. Ordog, Membrane-to-nucleus signaling links insulin-like growth factor-1- and stem cell factor-activated pathways, PLoS One 8 (2013) e76822.
[75] W. Zhao, J. Luo, S. Jiao, Comprehensive characterization of cancer subtype associated long non-coding rnas and their clinical implications, Sci. Rep. 4 (2014) 6591.
[76] J. Li, P.T. Li, W. Wu, B.N. Ding, Y.G. Wen, H.L. Cai, S.X. Liu, T. Hong, J.F. Zhang, J. D. Zhou, L.Y. Qian, J. Du, Pou2f2-mediated upregulation of lncrnaptprg-as1 inhibits ferroptosis in breast cancer via mir-376c-3p/slc7a11 axis, Epigenomics 16 (2024) 215–231.
[77] Q. Ma, R. Niu, W. Huang, L. Da, Y. Tang, D. Jiang, Y. Xi, C. Zhang, Long noncoding rna ptprg antisense rna 1 reduces radiosensitivity of nonsmall cell lung cancer cells via regulating mir-200c-3p/tcf4, Technol. Cancer Res. Treat. 19 (2020) 1079210263.
[78] Z. Shen, Y. Wu, G. He, Long non-coding rna ptprg-as1/microrna-124-3p regulates radiosensitivity of nasopharyngeal carcinoma via the lim homeobox 2-dependent notch pathway through competitive endogenous rna mechanism, Bioengineered 13 (2022) 8208–8225.
[79] L. Yi, L. Ouyang, S. Wang, S.S. Li, X.M. Yang, Long noncoding rna ptprg-as1 acts as a microrna-194-3p sponge to regulate radiosensitivity and metastasis of nasopharyngeal carcinoma cells via prc1, J. Cell Physiol. 234 (2022) 19088–19102.
[80] R. Ge, P. Yang, B. Wen, Upregulation of long-noncoding rna ptprg-as1 can predict the poor prognosis and promote migration and invasion in patients with osteosarcoma, Oncol. Lett. 21 (2021) 464.
[81] H.B. Binang, Y.S. Wang, M.A. Tewara, L. Du, S. Shi, N. Li, A.G.A. Nsenga, C. Wang, Expression levels and associations of ve long non-coding rnas in gastric cancer and their clinical signi cance, Oncol. Lett. 19 (2021) 2431.
[82] Z. Jiang, J. Guo, B. Xiao, Y. Miao, R. Huang, D. Li, Y. Zhang, Increased expression of mir-421 in human gastric carcinoma and its clinical association, J. Gastroenterol. 45 (2010) 17–23.
[83] X. Jin, N. Yu, Microrna-421 gene polymorphism in gastric carcinoma, Med. Sci. Monit. 22 (2016) 1467–1471.
[84] R. Wang, S. Song, J. Qin, K. Yoshimura, F. Peng, Y. Chu, Y. Li, Y. Fan, J. Jin, M. Dang, E. Dai, G. Pei, G. Han, D. Hao, Y. Li, D. Chatterjee, K. Harada, M.P. Pizzi, A.W. Scott, G. Tatlonghari, X. Yan, Z. Xu, C. Hu, S. Mo, N. Shanbhag, Y. Lu, M. Sewastjanow-Silva, A.A. Fouad Abdelhakeem, G. Peng, S.M. Hanash, G.A. Calin, C. Yee, P. Mazur, A.N. Marsden, A. Futreal, Z. Wang, X. Cheng, J.A. Ajani, L. Wang, Evolution of immune and stromal cell states and ecotypes during gastric adenocarcinoma progression, Cancer Cell 41 (2023) 1407–1426.
[85] H. Liu, H. Wu, Y. Tseng, Y. Chen, D. Zhang, L. Zhu, L. Dong, X.Z. Shen, T.T. Liu, Serum microrna signatures and metabolomics have high diagnostic value in gastric cancer, BMC Cancer 18 (2018) 415.
[86] F.S. Manoel-Caetano, A.F.T. Rossi, G. Calvet De Morais, F.E. Severino, A.E. Silva, Upregulation of the ape1 and h2ax genes and mirnas involved in dna damage response and repair in gastric cancer, Genes Dis. 6 (2018) 176–184.